

A smoothed finite element method for exterior Helmholtz equation in two dimensions

Yingbin Chai^a, Zhixiong Gong^a, Wei Li^{a,b,c,*}, Tianyun Li^{a,b,c}, Qifan Zhang^a

^a School of Naval Architecture and Ocean Engineering, Huazhong University of Science and Technology (HUST), Wuhan, Hubei 430074, China

^b Collaborative Innovation Center for Advanced Ship and Deep-Sea Exploration (CISSE), Shanghai 200240, China

^c Hubei Key Laboratory of Naval Architecture & Ocean Engineering Hydrodynamics, Huazhong University of Science and Technology (HUST), Wuhan, Hubei 430074, China



ARTICLE INFO

Keywords:

Gradient smoothing technique (GST)
Unbounded domains
Numerical method
Helmholtz equation
Underwater acoustic scattering

ABSTRACT

In this work, a smoothed finite element method (SFEM), in which the gradient smoothing technique (GST) from meshfree methods is incorporated into the standard Galerkin variational equation, is proposed to handle the acoustic wave scattering by the obstacles immersed in water. In the SFEM model, only the values of shape functions, not the derivatives at the quadrature points, are required and no coordinate transformation is needed to perform the numerical integration. Due to the softening effects provided by the GST, the original “overly-stiff” FEM model has been properly softened and a more appropriate stiffness of the continuous system can be obtained, then the numerical dispersion error for the acoustic problems is decreased conspicuously and the quality of the numerical solutions can be improved significantly. To tackle the exterior Helmholtz equation in unbounded domains, we use the well-known Dirichlet-to-Neumann (DtN) map to guarantee that there are no spurious reflecting waves from the far field. Numerical tests show that the present SFEM-DtN works well for exterior Helmholtz equation and can provide better solutions than standard FEM.

© 2017 Elsevier Ltd. All rights reserved.

1. Introduction

The acoustic scattering from the objects immersed in fluid medium is a very interesting phenomenon and studying how the propagation of the acoustic wave is affected when an obstacle stands on its path is of great importance in many engineering applications such as non-destructive testing, underwater acoustics, sonar mine-hunting, particle manipulation and so on. It is known that the exact solutions of acoustic scattering from the objects with simple geometrical shapes (spheres or spheroids) can be obtained by several analytical or semi-analytical approaches, such as the separation of variables, the partial wave series expansions (PWSE) method [1], the Fourier matching method (FMM) [2] and the T-matrix method [3,4]. However, if the objects is relatively complicated and with arbitrary shapes, it may be almost impossible or extremely difficult to handle the acoustic scattering problems using the above-mentioned approaches. In order to overcome this, we have to resort to the numerical techniques.

In recent years, with the extensive applications of the computer techniques, many numerical methods have been widely employed in various engineering practice. Foremost among these are the boundary element method (BEM) and the finite element method (FEM). As is known to all, the two methods are the most powerful and well-developed nu-

merical techniques for acoustic scattering problems. The boundary element method, which can be regarded as a boundary-based method, has obvious advantages in solving the acoustic scattering problems in unbounded domains. In BEM, only boundary discretization is required and the radiation condition (or Sommerfeld radiation condition) at infinity is obeyed naturally. Therefore, the number of equations to be solved can be notably reduced by using BEM to tackle the involved boundary-value problems. However, the BEM is also known to encounter several difficulties in coping with the exterior Helmholtz problems [5]: first, the obtained system matrices from BEM are non-symmetric and dense, which is opposed to the FEM (the corresponding matrices are symmetric and sparse). This will significantly increase the processing time of BEM for the acoustic problems. Second, in the classical BEM, the numerical solutions to the continuous boundary integral equations are always not unique at certain characteristic wave number values. More importantly, the distribution of these special wave number values, at which the nonunique solutions can be obtained, will be progressively more dense with the increase of the wave number range. In order to deal with this difficulty, some special treatments should be adopted. In addition, the classical BEM is relatively limited in solving the boundary-value problems in nonisotropic and nonhomogeneous media. In recent years, a novel singular boundary method (SBM) [6–9] has been proposed to

* Corresponding author at: School of Naval Architecture and Ocean Engineering, Huazhong University of Science and Technology (HUST), Wuhan, Hubei 430074, China.

E-mail address: hustliw@hust.edu.cn (W. Li).

handle the acoustic radiation and acoustic scattering problems. In SBM, the concept of source factor is introduced to regularize the singularities of the fundamental solutions. The SBM successfully overcomes some drawbacks of the original BEM. Nevertheless, the mathematical theoretical analysis of the SBM seems to be not sufficiently complete and the relevant work is still on its way.

An effective alternative to the classical BEM is the finite element method (FEM). The FEM, as opposed to the BEM, is a typical domain-based numerical technique. It is formulated from the variational principle and the convergence of the FEM solutions to the exact ones for Helmholtz problems has been well-proved. Based on the firm mathematical background, the classical FEM is capable of solving the Helmholtz problems with arbitrary large wave number values as long as the sufficiently fine mesh is employed. In addition, the FEM is not restricted to the problems in the nonisotropic and nonhomogeneous media, and the coupling with complex structures can be performed naturally by using FEM. Unfortunately, the standard Galerkin FEM also suffers from some inherent deficiencies. In general, the FEM solutions of the Helmholtz equation are always affected by the numerical errors [10]. It has been proved that these numerical errors could be decomposed into two kinds of components, namely the interpolation error and the dispersion error (or pollution error) [10]. When the FEM is employed to solve the Helmholtz problems, the interpolation error always arises and it is associated with the ability of the FEM to approximate the exact solution. For standard elasticity and thermal problems, the numerical error of the FEM solutions is exactly the interpolation error. This kind of numerical error is local and it will converge at the same rate by reducing the mesh size. For Helmholtz problems, the interpolation error can be controlled by keeping $kh = \text{constant}$ (where h is the average mesh size and k is the wave number). This is the well-known “rules of thumb”. According to this criterion, the minimum elements (at least six elements are required in general) should be used to discretize a wavelength. This means that the used meshes should get finer when the wave number values get larger. In the contrast to the interpolation error, the pollution error, which is associated with the phase error of the FEM solutions, is global and cannot be eliminated by refining the local meshes. Whether the “rules of thumb” is satisfied or not, the pollution effect exists all the same. More importantly, the pollution error is relatively small and can be neglected for small wave number values. With the increase of the wave number values, the pollution error will grow drastically and dominate the total error. As a consequence, even though the “rules of thumb” is followed, the standard FEM can only obtain relatively reliable solutions for small wave number values and cannot provide sufficiently accurate solutions for large wave number values.

In order to enhance the performance of the standard FEM and improve the accuracy of the FEM solutions for Helmholtz problems, a number of modified FEMs, extended FEMs and meshless techniques have been developed to address the pollution error in the past few decades. These methods include the generalized FEM (GFEM) [11], the Galerkin/least-squares FEM (GLS-FEM) [5], the radial point interpolation method (RPIM) [12] and the element-free Galerkin method (EFGM) [13]. Although all of these new numerical techniques could control the pollution effect in Helmholtz problems with varying degree of success, none of them can remove the pollution effects completely. To the author's best knowledge, the optimal numerical method to control the pollution effects has not been found at present and the quest for this will continue.

As mentioned in Ref. [14], the pollution error of the FEM solutions for the Helmholtz equation may mainly result from the approximate discrete model. Due to the inherent properties of the standard FEM, the obtained stiffness of the continuous system always behaves stiffer than the exact one, and then the pollution effects will arise. Therefore, producing a more proper and softer stiffness for the discrete model provides us another way to control the pollution effects. In recent years, Liu and his colleagues proposed the novel weakened weak form (or W^2) based

on the G space theory [15,16]. Using the W^2 form and the gradient smoothing technique from the meshless methods, the smoothed point interpolation methods (S-PIMs) [17–21] have been proposed to solve the partial differential equations in solid mechanic problems. As a particular form of the S-PIMs, a series of smoothed finite element methods (SFEMs) [22–30] were developed by Liu's et al. recently. In contrast to point interpolation method [31,32] and smoothed particle hydrodynamics (SPH) [33–35] method, which are the typical meshless techniques [36], the SFEM reserves both the good properties of the meshless techniques and the good properties of the standard FEM. Due to the softening effects provided by the W^2 form and the GST, the system stiffness from S-FEM behaves softer than that from the standard FEM and is closer to the exact one. Therefore, more accurate numerical solutions can be obtained from the SFEM compared to the “overly-stiff” FEM. The SFEM was initially employed to deal with the linear elastic solid mechanic problems [37–41]. Owing to the good and attractive properties, the SFEM has been applied to many other fields [42–52]. Recently, the SFEMs also have extended to solve the acoustic and structural-acoustic problems [53–61]. It is demonstrated that the pollution error of the FEM solutions for Helmholtz problems has been substantially controlled by the SFEM.

It is known that many mechanisms and physical phenomena of exterior acoustic problems (acoustic scattering or acoustic radiation) are quite different from the interior acoustic problems. Actually, some physical parameters of the scatterer (such as the shape of the scatterer) are generally presented in the signals carried by the returning backscattering waves. It is possible to extract some important geometrical information of the scatterer by studying the acoustic scattered field (practically, these are exactly the fundamental steps to perform the acoustical imaging of the underwater objects). This is very meaningful in many practical engineering applications such as sonar mine-hunting and sonar detection in ocean acoustics. However, the precondition of performing the acoustical imaging operations is to exactly obtain the acoustic scattered field of the underwater objects.

The present paper aims at employing a smoothed finite element method with quadrilateral elements to deal with the acoustic scattering problems. Due to the good performance of the SFEM in solid mechanics and interior acoustic problems, it is reasonable to expect that the SFEM is effective to handle the acoustic scattering successfully and can provide better solutions than the standard FEM. To tackle the exterior Helmholtz equation in unbounded domains, we use the well-known Dirichlet-to-Neumann (DtN) map to guarantee that there are no spurious reflecting waves from the far field. Numerical tests show that the present SFEM cum DtN map (SFEM-DtN) can provide better solutions than the standard FEM and therefore has great potential in the practical engineering application of underwater acoustics. The remainder of the present paper is structured as follows: Next section presents the governing equations for the exterior Helmholtz problems. The finite element formulations for the exterior acoustic problems are retrospected in Section 3. Section 4 includes the detailed formulation of SFEM for acoustic problems. The numerical error assessment for the Helmholtz problems is given in Section 5. Several typical numerical examples are analyzed and discussed in Section 6, and the final conclusions are summarized in Section 7.

2. The description of the exterior Helmholtz equation

We consider the propagation of the acoustic wave is linear and harmonic, and the surrounding medium is quiescent and uniform. Then the acoustic wave is governed by the following partial differential equation:

$$\Delta P - \frac{1}{c^2} \frac{\partial^2 P}{\partial t^2} = 0 \quad (1)$$

in which Δ stands for the Laplace operator; P denotes the unknown acoustic pressure, c and t represent the speed of the acoustic wave and time, respectively.

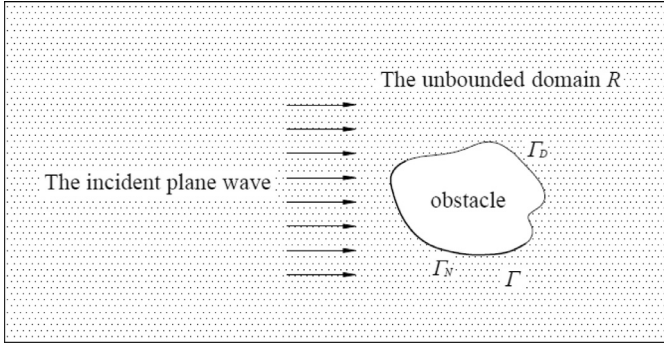


Fig. 1. The schematic illustration of the plane acoustic wave scattering by an object with arbitrary shapes.

Using the harmonic behavior of the acoustic wave, the acoustic pressure is given by

$$P(\mathbf{x}) = p(\mathbf{x}) \exp(j\omega t) \quad (2)$$

in which $p(\mathbf{x})$ denotes the amplitude of the acoustic pressure, ω represents the angular frequency, j is the imaginary unit.

Substituting Eq. (2) into Eq. (1), we have

$$\Delta p + k^2 p = 0 \quad (3)$$

in which k stands for the wave number which is associated with ω and c by $k = \omega/c$.

The above equation is the well-known reduced equation (or Helmholtz equation). By complementing a set of proper boundary conditions, Eq. (3) can be solved ultimately. In general, there are three kinds of boundary conditions for the Helmholtz equation, namely, the Dirichlet boundary condition (Γ_D), the Neumann boundary condition (Γ_N) and the Robin boundary condition (Γ_R). These boundary conditions can be described as follows:

$$p = p_D \quad \text{on } \Gamma_D \quad (4)$$

$$\frac{\partial p}{\partial n} = -j\rho\omega v_n \quad \text{on } \Gamma_N \quad (5)$$

$$\frac{\partial p}{\partial n} = -j\rho\omega A_n p \quad \text{on } \Gamma_R \quad (6)$$

in which n is the unit outward normal vector to the corresponding boundary, ρ is the density of the medium, v_n is the normal velocity on Γ_N and A_n is the admittance coefficient on Γ_R .

From the above equation, it can be found that: on the Dirichlet boundary condition Γ_D , the acoustic pressure p is equal to the prescribed values p_D ; on the Neumann boundary Γ_N , the normal velocity v is prescribed to be a given value v_n ; on the Robin boundary condition, the normal velocity is prescribed to be proportional to the acoustic pressure. For the acoustic scattering problems in the unbounded domains (see Fig. 1), we have

$$\Delta p + k^2 p + f = 0 \quad \text{in } R \quad (7)$$

$$p = g \quad \text{on } \Gamma_D \quad (8)$$

$$\frac{\partial p}{\partial n} = q \quad \text{on } \Gamma_N \quad (9)$$

$$\lim_{r \rightarrow \infty} r^{\frac{(d-1)}{2}} \left(\frac{\partial p}{\partial r} - jkp \right) = 0 \quad (10)$$

in which f denotes the acoustic source term, g and q are the prescribed function, r denotes the distance from the origin and d is the spatial dimension, R represents the involved unbounded problem domain and it

is internally bounded by the boundary Γ of the object, the boundary Γ is assumed to be piecewise smooth and it is delimited by $\Gamma = \Gamma_D \cup \Gamma_N$, and $\Gamma_D \cap \Gamma_N = \emptyset$, in which Γ_D and Γ_N are the relevant boundary condition defined in previous context.

Eq. (10) represents the well-known Sommerfeld radiation condition. It should be obeyed so that there are no spurious reflecting waves from the far field and the solution to the boundary-value problem defined by Eqs. (7)–(10) is unique. In addition, it should be pointed out that the above-defined boundary-value problem cannot be solved directly by using the conventional domain-based numerical techniques (such as the classical FEM) because the involved problem domain is unbounded. In general, this difficulty can be circumvented by introducing an artificial boundary, which truncates the original unbounded domain and yields a bounded computational domain. The related formulation will be given in the next section.

3. Finite element formulation for the exterior Helmholtz equation

An artificial boundary is generally introduced to enable the conventional FEM to cope with the exterior Helmholtz problems in unbounded domains. As shown in Fig. 2, the original unbounded region R is decomposed into two parts by the artificial boundary B , namely, the internal bounded domain Ω_I and the residual external domain Ω_O which is still unbounded. The bounded domain Ω_I , which is externally bounded by the artificial boundary B and internally bounded by the surface of the object, contains all the material inhomogeneity, source terms and geometric irregularities within it. The problem in the external unbounded domain can be regarded as a typical exterior boundary-value problem and it can be solved by the analytical approach. In order to obtain the corresponding analytical solution easily, the artificial boundary B (often a d -dimensional sphere) is generally constructed as simple as possible. After obtaining the analytical solution to this exterior boundary-value problem, the relationship between the function (the Dirichlet datum) and its normal derivative (the Neumann datum), which is also called the Dirichlet-to-Neumann (DtN) map, can be obtained naturally. This is the exact impedance on the artificial boundary B for the problem in the internal bounded domain Ω_I . By imposing the DtN map on the B , the problem in Ω_I can be solved successfully using the conventional domain-based numerical techniques. Then the numerical solution in the entire original region can be obtained ultimately.

Following these ideas, Eq. (10) will be replaced by the following equation for the above boundary-value problem.

$$\frac{\partial p}{\partial n} = -Mp \quad \text{on } B \quad (11)$$

in which M is the DtN map and it relates the acoustic pressure p to its normal derivative $\frac{\partial p}{\partial n}$ on the artificial boundary B .

It is worth noting that the definition of M is not dependent on the acoustic pressure and its normal derivative. It can be derived from the analytical solution of the boundary-value problem defined in the residual external domain Ω_O . According to Keller and Givoli [62], the corresponding solution in two-dimensional space is given by

$$p(r, \theta) = \frac{1}{\pi} \sum_{n=0}^{\infty} ' \int_0^{2\pi} \frac{H_n^{(1)}(kr)}{H_n^{(1)}(kR)} \cos n(\theta - \theta') p(R, \theta') d\theta' \quad (12)$$

where R is the radius of the circular artificial boundary, $p(R, \theta')$ is the prescribed Dirichlet data on the artificial boundary, $H_n^{(1)}$ is the Hankel function of the first kind with n order, the prime after the sum means that the corresponding value is halved for the first term.

By differentiating Eq. (12) with respect to the argument r , we have

$$p_v = \frac{\partial p(r, \theta)}{\partial n} |_{r=R} = - \sum_{n=0}^{\infty} ' \int_0^{2\pi} m_n(\theta - \theta') p(R, \theta') d\theta' \quad (13)$$

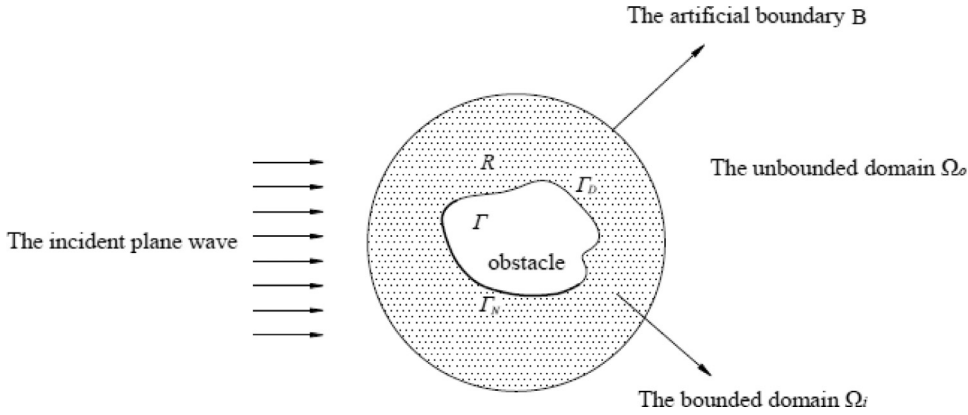


Fig. 2. The artificial boundary B for the exterior Helmholtz problems.

in which p_v is the normal derivative of the acoustic pressure on B and the coefficient $m_n(\theta - \theta')$ is given by

$$m_n(\theta - \theta') = -\frac{k}{\pi} \frac{H_n^{(1)'}(kR)}{H_n^{(1)}(kR)} (\cos n\theta \cos n\theta' + \sin n\theta \sin n\theta') \quad (14)$$

Then the explicit expression of the DtN operator M can be obtained by substituting Eqs. (12) and (13) into Eq. (11).

After having obtained the DtN operator M , we will start to derive the standard Galerkin weak form of the above boundary-value problem. According to Harari and Hughes [5], this boundary-value problem can be defined by: Find $p \in S$ such that $\forall w \in V$ (where S represents the trial solutions space and V denotes the weighting functions space)

$$a(w, p) + b(w, p) = (w, f)_\Omega + (w, q)_\Gamma \quad (15)$$

where

$$a(w, p) = \int_\Omega (\nabla w \nabla p - k^2 w p) d\Omega \quad (16)$$

$$b(w, p) = - \int_B w \frac{\partial p}{\partial n} d\text{B} \quad (17)$$

$$(w, f)_\Omega = \int_\Omega w f d\Omega \quad (18)$$

$$(w, q)_\Gamma = \int_{\Gamma_N} w q d\Gamma \quad (19)$$

By substituting Eqs. (11)–(13) into Eq. (17), the corresponding weak form of this boundary-value problem can be obtained easily.

Assuming that the solution of the acoustic pressure can be approximated in terms of the following form

$$p = \sum N_i p_i = \mathbf{N} \mathbf{p} \quad (20)$$

in which p_i is the unknown acoustic pressure associated with node i and N_i is the corresponding FEM shape functions.

By substituting Eqs. (8)–(9) and Eq. (20) into Eq. (15), and using the Green's formula, the discretized equation for the exterior Helmholtz equation can be re-written in the following matrix form

$$[\mathbf{K} - k^2 \mathbf{M} + \mathbf{K}_{AB}^b] [\mathbf{P}] = [\mathbf{F}] \quad (21)$$

in which \mathbf{K} and \mathbf{M} are the so-called acoustical stiffness matrix and the acoustic mass matrix, respectively.

$$\mathbf{K} = \int_\Omega (\nabla \mathbf{N})^T \nabla \mathbf{N} d\Omega \quad (22)$$

$$\mathbf{M} = \int_\Omega \mathbf{N}^T \mathbf{N} d\Omega \quad (23)$$

and \mathbf{P} and \mathbf{F} represent the acoustic pressure associated with the nodes in the problem domain and the nodal force vector, respectively.

$$[\mathbf{P}]^T = [p_1, \quad p_2, \quad \dots, \quad p_n] \quad (24)$$

$$\mathbf{F} = -j\rho\omega \int_{\Gamma_N} \mathbf{N}^T v_n d\Gamma \quad (25)$$

In Eq. (21), \mathbf{K}_{AB}^b denotes the matrix which is associated with the DtN map and can be given by

$$\begin{aligned} \mathbf{K}_{IJ}^b &= \int_B \mathbf{N}_I M \mathbf{N}_J d\Omega = - \sum_{j=0}^{\infty} \frac{k}{\pi} \frac{H_n^{(1)'}(kR)}{H_n^{(1)}(kR)} \left(\int_B \mathbf{N}_I(\mathbf{x}) F_j(\mathbf{x}) d\Omega \right) \\ &\quad \times \left(\int_B \mathbf{N}_J(\mathbf{x}) F_j(\mathbf{x}') d\Omega \right) \end{aligned} \quad (26)$$

where \mathbf{N}_I and \mathbf{N}_J denote the corresponding shape functions associated with node I and J , the simple trigonometric functions $F_j(\mathbf{x})$ and $F_j(\mathbf{x}')$ are given by

$$F_j(\mathbf{x}) = [\cos n\theta \quad \sin n\theta] \quad (27)$$

$$F_j(\mathbf{x}') = \begin{bmatrix} \cos n\theta' \\ \sin n\theta' \end{bmatrix} \quad (28)$$

From Eq. (21), it is interesting to note that the influence of the DtN map on the original finite element formulation for the exterior Helmholtz equation is the inclusion of the additional matrix \mathbf{K}_{AB}^b and only the related numerical integration along the boundary B is required to form the matrix \mathbf{K}_{AB}^b . This helps to incorporate the DtN map into the original finite element formulation for the exterior Helmholtz equation. In addition, due to the non-local property of the DtN map, the matrix \mathbf{K}_{AB}^b is not sparse and banded in general. This may increase the bandwidth and spoil the sparseness of the original acoustic stiffness \mathbf{K} . However, the original bandwidth and sparseness of the matrix \mathbf{K} can be maintained by carefully ordering the number of nodes on the artificial boundary. Numerical tests show that the DtN map is quite effective to handle the exterior Helmholtz problems.

Additionally, it should be pointed out that the DtN map in the above formulation is denoted by infinite terms. In the view of numerical computation, it is impractical to perform the full DtN map and it should be truncated at some limit (at a maximum limit n_{\max}). Moreover, the radius of the artificial boundary B is also a crucial parameter in performing the DtN map. Actually, the larger values of the radius R as well as the parameter n_{\max} are helpful to improve the accuracy of the numerical solution. If the value of R is not sufficiently large, the quality of the numerical solution will degrade substantially due to the largish round-off errors. However, large values of R will significantly increase the computational demands. On the other hand, using the truncated DtN map

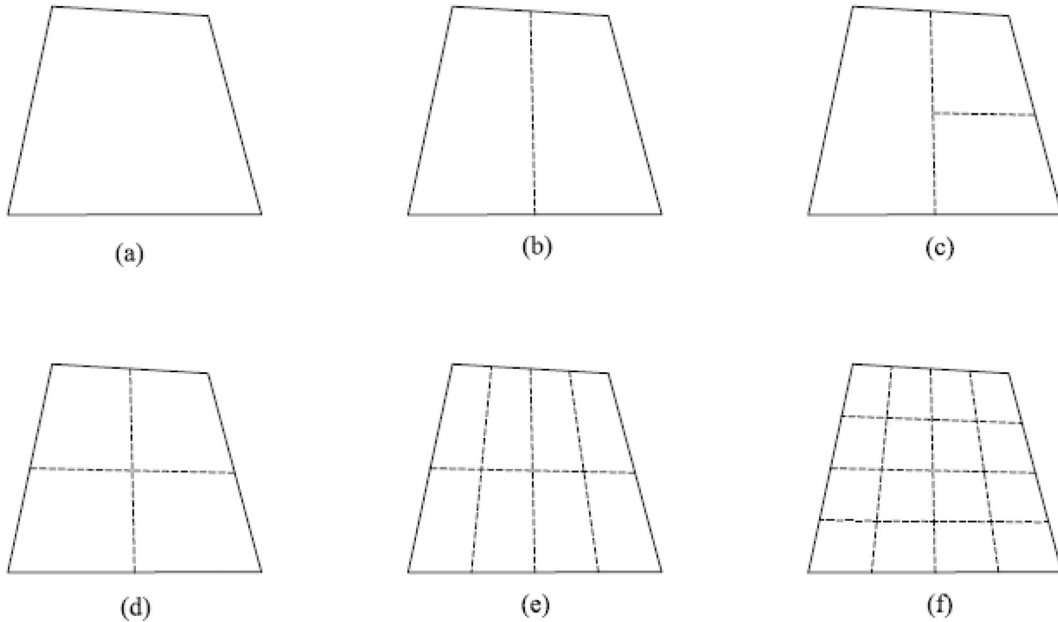


Fig. 3. The original quadrilateral element Ω_i^e is divided into $n_e^s \in [1, +\infty]$ smoothing domains by linking the mid-points of the opposite segments: (a) 1SD; (b) 2SDs; (c) 3SDs; (d) 4SDs; (e) 8SDs; (f) 16 SDs.

always lead to the truncation error and this kind of error will become smaller with the increase of the parameter n_{\max} . According to Keller and Givoli [62], there exists an optimal n (n_{opt}) for the average mesh size h and the fixed R . This value of n_{opt} occurs when the finite element discretization error equals the truncation error. According to Ref. [62], the optimal n (n_{opt}) and the value of R satisfies the following formula:

$$n_{\text{opt}} = -(l+1) \frac{\log_{10}(h)}{\log_{10}(R)} \quad (29)$$

in which l denotes the degree of the used polynomial FEM shape functions.

From a number of numerical tests, it is found that the above formula is very reasonable and effective to determine the values of the two parameters though it is a crude estimate. In this work, unless otherwise specified, we directly use $n_{\max} = 40$ and $R = 1.2$ to perform the practical computation for all the numerical examples. Numerical results show that the above values of the two parameters are sufficient to guarantee the quality of the numerical solutions.

4. Brief of the SFEM for acoustic problems

In SFEM, the initial quadrilateral elements are identical to those used in the standard FEM such that $\Omega = \cup_{i=1}^{N^e} \Omega_i^e$ and $\Omega_i^e \cap \Omega_j^e = \emptyset$, $i \neq j$ (where Ω is the problem domain, Ω_i^e is the quadrilateral element, N^e is the number of the used elements). In order to perform the gradient smoothing technique, the related smoothing domain (SD) should be obtained first. As shown in Fig. 3, each quadrilateral element Ω_i^e is further divided into $n_e^s \in [1, +\infty]$ sub-quadrilateral elements by linking the mid-points of the opposite segments such that $\Omega_i^e = \cup_{m=1}^{n_e^s} \Omega_{i,m}^s$ (where $\Omega_{i,m}^s$ stands for the smoothing domain). As a consequence, the total involved problem domain is divided into $N_s = N^e \times n_e^s$ nonoverlapping and no-gap SDs, then the gradient field will be smoothed by performing the gradient smoothing technique over these SDs.

For each smoothing domain Ω^s , the smoothed acoustical stiffness matrix is obtained by

$$\mathbf{K}^s = \int_{\Omega^s} (\bar{\nabla} \mathbf{N})^T (\nabla \mathbf{N}) d\Omega \quad (30)$$

For the Helmholtz problems, the gradient of the acoustic pressure is associated with the acoustic particle velocity and can be expressed by

$$\nabla p + j\rho\omega v = 0 \quad (31)$$

In this paper, the acoustic particle velocity v is smoothed by the gradient smoothing technique in the present formulation and the smoothed acoustic particle velocity $\bar{v}(\mathbf{x})$ in each smoothing domain Ω^s is given by

$$\bar{v}(\mathbf{x}) = \int_{\Omega^s} v(\mathbf{x}) \Phi(\mathbf{x}) d\Omega \quad (32)$$

in which $\Phi(\mathbf{x})$ is a positive smoothing function which should possess the following property

$$\int_{\Omega^s} \Phi(\mathbf{x}) d\Omega = 1 \quad (33)$$

In general, the smoothing function $\Phi(\mathbf{x})$ is taken as

$$\Phi(\mathbf{x}) = \begin{cases} \frac{1}{A^s} \mathbf{x} \in \Omega^s \\ 0 \mathbf{x} \notin \Omega^s \end{cases} \quad (34)$$

in which $A^s = \int_{\Omega^s} d\Omega$ is the area of the smoothing domain Ω^s .

Using the divergence theorem and substituting Eq. (31) into Eq. (32), the smoothed acoustic particle velocity can be re-written by

$$\bar{v}(\mathbf{x}) = -\frac{1}{j\rho\omega A_k^s} \int_{\Omega^s} \nabla p d\Omega = -\frac{1}{j\rho\omega A_k^s} \int_{\Gamma^s} p \cdot \mathbf{n} d\Gamma \quad (35)$$

in which Γ^s denotes the boundary of the smoothing domain Ω^s and \mathbf{n} is a matrix which contains the components of the outward normal vector to the boundary Γ^s .

$$\mathbf{n} = \begin{bmatrix} n_x \\ n_y \end{bmatrix} \quad (36)$$

From Eq. (35), it is evident that the area integration over the smoothing domain Ω^s becomes the line integration along the boundary Γ^s in the process of performing the gradient smoothing operation.

Using the finite element approximation form (Eq. (20)) of the acoustic pressure, the smoothed version of the acoustic particle velocity can be obtained by

$$\bar{v}(\mathbf{x}) = -\frac{1}{j\rho\omega} \sum_{i \in M_k} \bar{\mathbf{B}}_i(\mathbf{x}) p_i \quad (37)$$

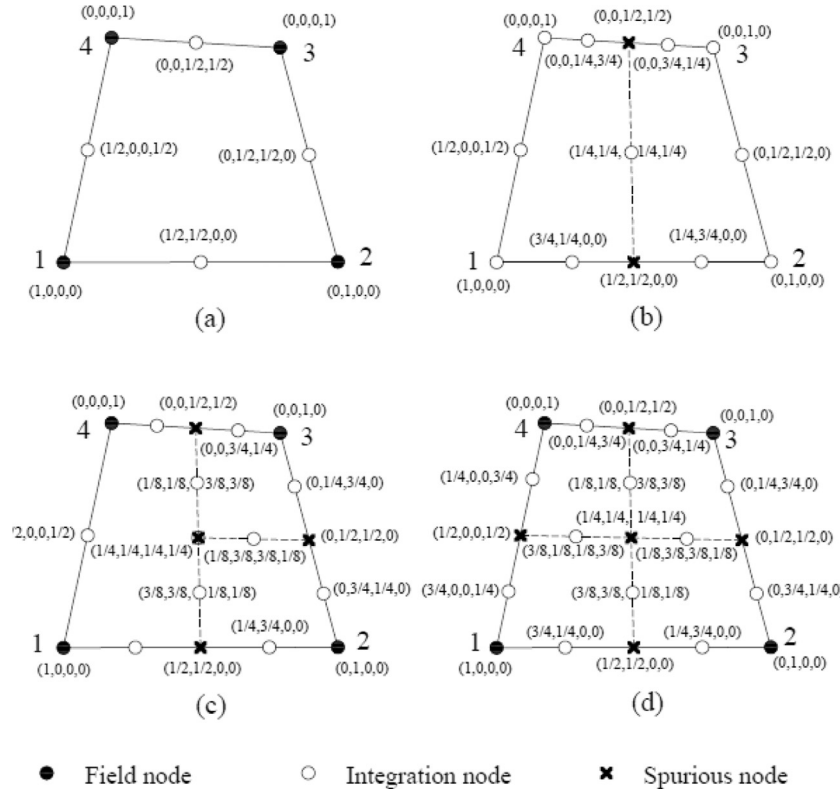


Fig. 4. The shape function values at the quadrature point distributed along the boundary of the smoothing domains: (a) 1SD; (b) 2SDs; (c) 3SDs; (d) 4SDs.

in which $\tilde{\mathbf{B}}_i(\mathbf{x})$ denotes the smoothed gradient matrix and M_k represents the number of involved nodes in the smoothing domain.

Using the Gauss integration scheme, the smoothed gradient matrix $\tilde{\mathbf{B}}_i(\mathbf{x})$ can be calculated by

$$\tilde{\mathbf{B}}_i(\mathbf{x}) = \frac{1}{A^s} \int_{\Gamma^s} \mathbf{N}_I(\mathbf{x}) \mathbf{n} d\Gamma = \frac{1}{A^s} \sum_{q=1}^{N_{se}} \left(\sum_{r=1}^{N_{GP}} w_{GP} \mathbf{N}_I(\mathbf{x}_{GP}) \mathbf{n} \right) \quad (38)$$

in which N_{se} is the number of segments in the boundary Γ^s , \mathbf{x}_{GP} is the position of the Gauss point, N_{GP} is the number of in each segment, w_{GP} is the corresponding weighting coefficients.

From Eq. (38), it is found that only the shape function values (not the derivatives of the shape function) at the Gauss points are required to perform the related numerical integration. Therefore, it is allowed to construct the shape function in a more flexible way. For the quadrilateral elements (Q4) used in this paper, the conventional bilinear shape functions are employed and the shape function values at the Gauss point can be evaluated easily. All required shape function values at the quadrature points are exhibited in Fig. 4. For the convenience of notation, the format (N_1, N_2, N_3, N_4) is used in the figure.

In addition, it should be pointed out that the related gradient smoothing operations used in the present SFEM-Q4 is quite different from the edge-based smoothed FEM with triangular elements (ES-FEM-T3) for acoustic scattering problems [60]. In the ES-FEM-T3, the corresponding edge-based smoothing domains are formed by sequentially linking the terminal points of each edge and the centers of the neighboring elements, while in the present SFEM-Q4, the process of obtaining the sub-smoothing domains is based on the original element itself. In this work, a simple division of the quadrilateral elements (Q4) into four sub-smoothing domains is performed. As a result, the bandwidth of the global system matrices (such as the stiffness matrix) for ES-FEM-T3 is always larger than that for standard FEM-T3. The reason for this is that only the nodes belonging to the mutual element is needed to assemble the global system matrices in FEM-T3. However, in term of the ES-FEM-T3, more node information (they may not belong to one triangular el-

ement) is needed to obtain the element stiffness matrix. Therefore, the bandwidth of the global stiffness matrix for ES-FEM-T3 is always larger than that for FEM-T3. While in the SFEM-Q4, the bandwidth of the system matrix is not increased compared to the FEM-Q4 because the gradient smoothing operations are performed over the original quadrilateral elements themselves (no neighboring elements are involved). Actually, the bandwidth of the system matrix for SFEM-Q4 is also always smaller than the ES-FEM-T3 with the same node distributions. This may result in that the SFEM-Q4 will possess higher computational efficiency than the ES-FEM-T3 for acoustic scattering problems, this point will be demonstrated by the related numerical example in Section 6.

After having obtained the smoothed gradient matrix, the smoothed stiffness matrix for the smoothing domain Ω^s can be given by

$$\bar{\mathbf{K}}_s = \int_{\Omega^s} \tilde{\mathbf{B}}^T \tilde{\mathbf{B}} d\Omega = \tilde{\mathbf{B}}^T \tilde{\mathbf{B}} A^s \quad (39)$$

Finally, the global smoothed stiffness matrix for the full problem domain can be assembled by

$$\bar{\mathbf{K}} = \sum_{s=1}^{N_s} \bar{\mathbf{K}}_s \quad (40)$$

Then the Helmholtz problems can be solved by the SFEM in the similar way as the standard FEM.

It is worth noting that the present SFEM has been proven to be variationally consistent if each quadrilateral element contains only one smoothing domain ($n_e^s = 1$) [22]. In this case, the numerical solutions from SFEM possess the same properties as those from the FEM using the reduced integration. Actually, the SFEM ($n_e^s = 1$) usually overestimate the solution of the real system for solid mechanic problems and the obtained numerical solution is usually the upper bound solution. However, with the increase of the value of n_e^s , the solution from SFEM ($n_e^s > 1$) will gradually approach the solution from the standard compatible FEM using the full integration and the lower bound solution can be obtained as long as the sufficiently large value of n_e^s is used. More importantly, the process of the changing the solution from upper to lower bound is

monotonic with the increasing n_e^s values. This means that there exists an optimal value of n_e^s which will result in the optimal numerical solutions. For the acoustic problem considered in this paper, the computational experience suggests that $n_e^s = 4$ can usually provide stable solutions and the obtained results are closest to the exact ones in almost all the cases. Therefore, $n_e^s = 4$ (see Fig. 4d) is used for all the numerical examples in this work.

5. Numerical error assessment for Helmholtz equation

It is well-known that the finite element approximations of the Helmholtz equation suffers from the numerical error issue which can be regarded as the difference between the wave number k' from the numerical techniques and the exact wave number k^e . In general, this numerical error will expand with the increase of the wave number values and cannot be removed completely even if the sufficiently fine meshes are employed. The effect of the numerical error has been extensively addressed in the past few decades. The rule of thumb is a simple and usual criterion to control the numerical error. In this criterion, a fixed number of elements should be used to resolve a wavelength. Numerical results show that this criterion indeed can control the numerical error to a certain extent. However, it is also widely known that this criterion only works well in the relatively small wave number range. For the large wave number range, it seems not very effective.

With the aim to assess the quality of the numerical solution for the Helmholtz equation, the numerical error indicator can be defined as [10]:

$$E_p = |p^e - p'|_1 = \int_{\Omega} (\tilde{v}^e - \tilde{v}')^T (v^e - v') d\Omega \quad (41)$$

in which the symbol “~” represents the complex conjugate of the corresponding variable, the superscript e and prime correspond to the exact solution and the solution from the numerical techniques, respectively.

It has been proved that the relative numerical error of the numerical solution can be bounded by the following equation [10]:

$$\eta = \frac{|p^e - p'|_1}{|p^e|_1} = \sqrt{\frac{\int_{\Omega} (\tilde{v}^e - \tilde{v}')^T (v^e - v') d\Omega}{\int_{\Omega} (\tilde{v}^e \cdot v^e) d\Omega}} \leq C_1 \left(\frac{kh}{l} \right)^l + C_2 k \left(\frac{kh}{l} \right)^{2l} \quad (42)$$

in which l stands for the degree of the polynomial shape function used in the numerical model, C_1 and C_2 are the related constants which do not depend on the average mesh size h and the wave number k .

Note that the shape functions used in this work are linear, hence Eq. (42) can be re-written by

$$\eta \leq C_1 kh + C_2 k^3 h^2 \quad (43)$$

It is shown that the total numerical error of the numerical solution can be decomposed into two different parts. The first part in Eq. (43) is the interpolation error. This kind of numerical error is associated with the ability of the discretized model to solve the continuous system and it can be controlled by keeping $kh = \text{constant}$. Actually, this error is local and it can be reduced by using the sufficiently fine meshes. The second part in Eq. (43) is the dispersion error (or pollution error). In contrast to the interpolation error, the dispersion error, which is associated with the phase difference between the numerical solutions and the exact ones, cannot be controlled by refining the used meshes. Compared to the interpolation error (which is related to kh), the dispersion error (which is related to $k^3 h^2$) has an additional dependence on the wave number k . This means that the related numerical error will accumulate with the increase of the wave number for the fixed mesh pattern. Whether the used meshes are sufficiently fine or not, the accumulation process of the dispersion error cannot be controlled. Besides, it is interesting to find that the rule of thumb mentioned in the previous section is practically used to control the interpolation error because using the fixed number of elements to resolve a wavelength is equivalent to keeping $kh = \text{constant}$.

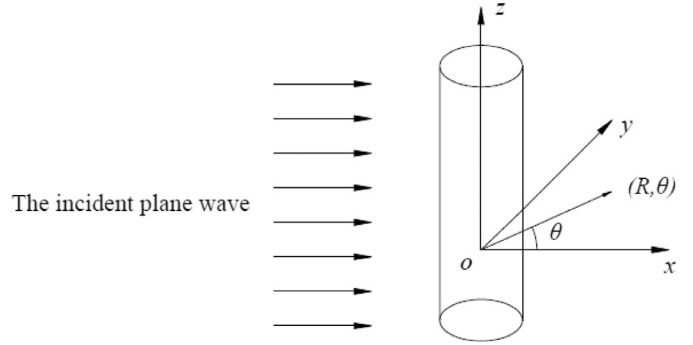


Fig. 5. The plane acoustic wave scattering by infinite cylinder with circular section.

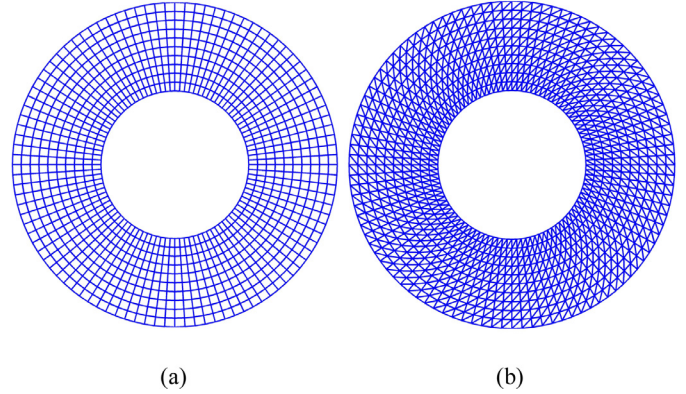


Fig. 6. The used meshes for the involved computational domain: (a) quadrilateral elements; (b) triangular elements.

From Eq. (43), it is obvious that this rule is not effective in controlling the dispersion error. In the present work, the exterior Helmholtz equation will be considered and the abilities of the standard FEM and the proposed SFEM in controlling the interpolation error and the dispersion error will be compared and discussed in detail.

6. Numerical examples

With the aim to validate that the present SFEM-Q4 is indeed effective and contributes to improve the accuracy of the original FEM-Q4 solutions for acoustic scattering problems, a number of typical numerical examples are considered in this section. The numerical solutions from the present SFEM-Q4 and some other numerical methods (FEM-Q4, FEM-T3 and ES-FEM-T3) will be compared and discussed, and then the validity and feasibility of the present SFEM-Q4 for acoustic scattering problems will be verified.

6.1. The acoustic scattering by infinite cylinder with circular section

The first considered numerical example is related to the plane acoustic wave scattering by infinite cylinder with circular section (see Fig. 5). The incident plane acoustic wave (the acoustic pressure amplitude is 1 Pa) is propagating along the x -axis and an infinite cylinder stands on its path. The radius of the cylinder is $a = 0.5$, the material parameters of the surrounding acoustic medium are chosen as density $\rho = 1000 \text{ kg/m}^3$ and acoustic wave speed $c = 1500 \text{ m/s}$. Note that all the variables are unchanged along the z -axis and one of the involved dimensions is much larger than the other two, this problem can be considered as a typical two-dimensional problem even if the three-dimensional space is involved. The unbounded problems domain is truncated by introducing a circular artificial boundary (radius $R = 1.2$) and the uniform quadrilateral elements and triangular elements (see Fig. 6) are used to discretize the obtained bounded computational domain. The exact solution to this

typical and simple acoustic scattering problem is easy to formulate and is given by

$$p = 2 \sum_{n=0}^{\infty}' \left[-(-j)^n \frac{\frac{d}{d(ka)} J_n(ka)}{\frac{d}{d(ka)} H_n^{(2)}(ka)} \right] H_n^{(2)}(kr) \cos(n\theta) \quad (44)$$

in which the prime after the sum means that the corresponding value is halved for the first term.

First, we will investigate how the accuracy of the present SFEM-Q4 solutions for acoustic scattering problems is affected by the number of the used smoothing domains. It is known that each original quadrilateral element can be divided into $n_e^s \in [1, +\infty]$ smoothing domains in the present SFEM-Q4 and the obtained stiffness of the system is monotonic with the increasing n_e^s values. For $n_e^s = 1$, the SFEM is exactly the FEM-Q4 using the reduced integration and the obtained numerical results are usually overestimated. On the other hand, if n_e^s trends to infinite, the present FEM-Q4 will become the standard compatible FEM using the full integration and the corresponding numerical results are usually underestimated. Therefore, it is indicated that there exists an optimal value of n_e^s which will result in the optimal numerical solutions. Here we will first determine the appropriate n_e^s for the acoustic scattering problems. For the wave number $k = 10$, the scattered acoustic pressure results at a distance of $R = 1$ m from the center of the artificial boundary versus the polar angle are shown in Fig. 7. To give a comparison, the SFEM-Q4 results using different smoothing domains together with other numerical results are also plotted in the figure. From the figure, we can see that the SFEM-Q4 results with 1SD is non-converge. The possible reason for this may be that the obtained system stiffness is overly softened if only one smoothing domain is used in each quadrilateral element and the corresponding numerical results are not sufficiently stable. With the increase of the value of n_e^s , the SFEM-Q4 results will become stable and approach the compatible FEM results using full integration. In addition, it is also seen that the SFEM-Q4 results with 4SD is closest to the exact solutions. Actually, from a plenty of numerical tests, it is found that $n_e^s = 4$ could always provide fairly good results for acoustic problems. Therefore, $n_e^s = 4$ is employed in this work for all the numerical examples.

6.1.1. The accuracy study

Here the accuracy of the present SFEM-Q4 for acoustic scattering problems will be studied by computing and discussing the corresponding numerical results from different numerical methods (FEM-T3, FEM-Q4, ES-FEM-T3 and SFEM-Q4). In order to take the wave number into consideration, several different dimensional wave numbers ($k = 3$, $k = 6$ and $k = 10$) are considered here. The scattering patterns of acoustic pressure solutions at different wave numbers are given in Fig. 8. For the convenience of exhibition, the acoustic pressure solutions at a distance of $R = 1$ m from the center of the artificial boundary are considered here. In order to give a comparison, the analytical solutions together with the numerical solutions from the four different approaches using the identical node distributions are plotted in the figures. From the results shown in the figures, we can clearly find that:

- (1) At small wave number ($k = 3$), the solutions from all the four mentioned numerical approaches have similar accuracy and are in very good agreement with the analytical solutions for the acoustic scattering problems.
- (2) With the increase of the considered wave number values, the performance of the numerical approaches will deteriorate progressively and the corresponding numerical solutions will deviate from the analytical solutions gradually. Though the SFEM-Q4 is not clearly better than the ES-FEM-T3 because they have very similar accuracy; however, the present SFEM-Q4 still shows much more excellent performance than the FEM-T3 and FEM-Q4, and the SFEM-Q4 results are obviously superior to the results from these two numerical techniques.

The above findings show that the present SFEM-Q4 is an effective alternative to the ES-FEM-T3 and also is feasible to handle the acoustic

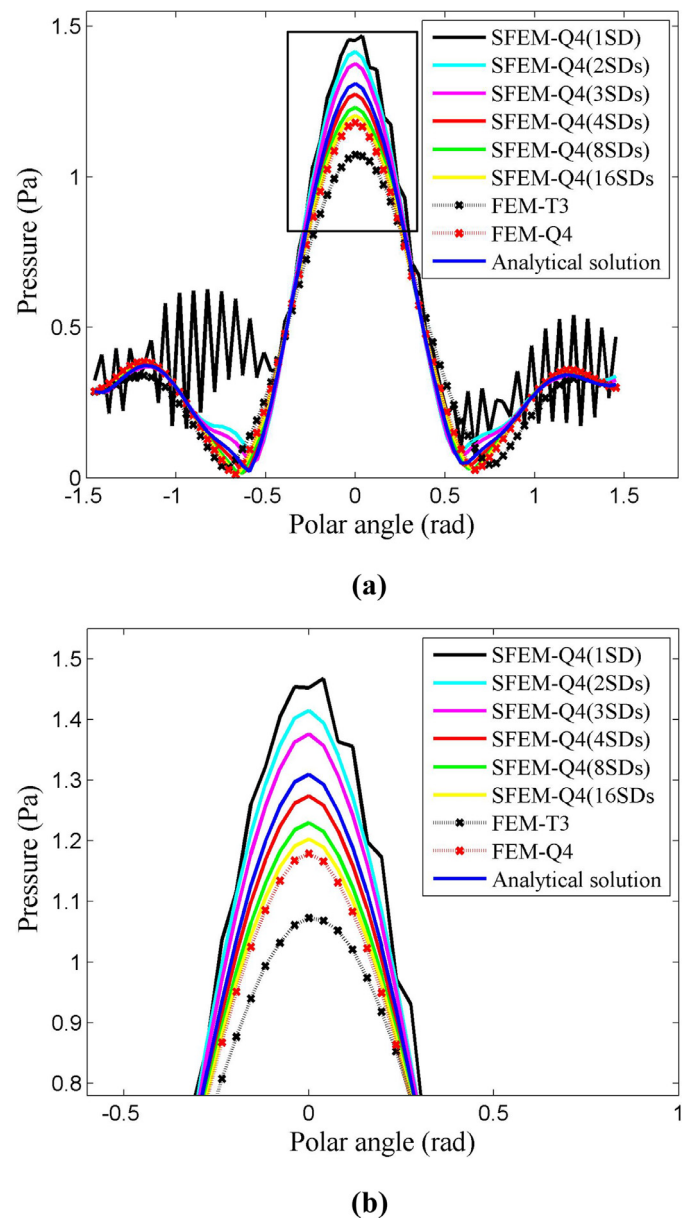
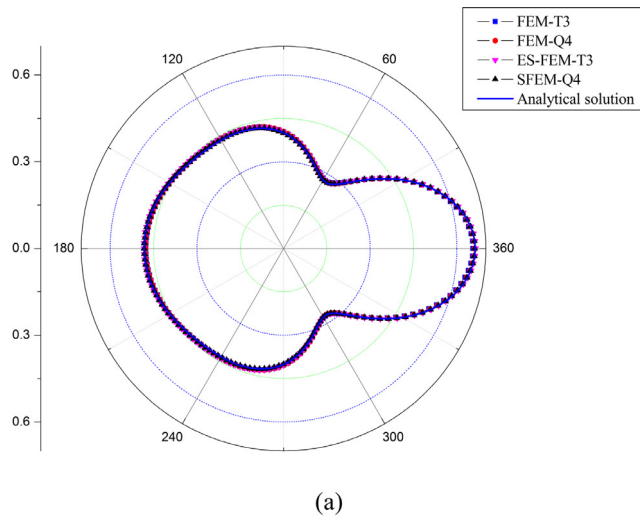


Fig. 7. The scattered acoustic pressure results along the artificial boundary versus the polar angle: (a) full scale distribution; (b) zoomed-in distribution.

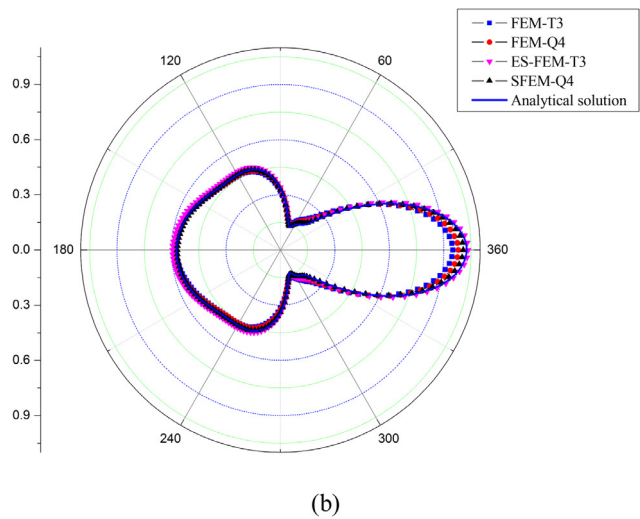
scattering problems. In addition, the performance of the original FEM-Q4 has been significantly improved by the present SFEM-Q4 due to the used gradient smoothing technique (GST).

6.1.2. The effects of nodal irregularity

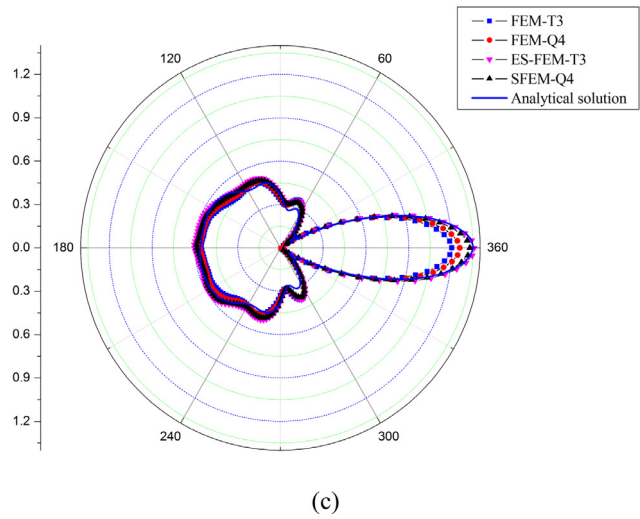
In the formulation of the standard isoparametric elements, one crucial step is the coordinate transform process. The natural coordinate system is associated with the physical coordinate system by this transform process and the mapping operations are required. With the aim to ensure the correspondence property of the transform process, only the convex elements (not the concave elements) are permitted in general. Actually, the standard FEM-Q4 elements are fairly sensitive to the mesh distortion and the accuracy of the obtained numerical solutions will usually degrade if the severely distorted meshes are used. In this sub-section, the influence of mesh distortion on the quality of the numerical solutions from different approaches will be investigated and discussed. Fig. 9 shows the used irregular mesh. The irregular mesh is generated from the



(a)



(b)



(c)

Fig. 8. The scattering patterns of acoustic pressure solutions at different wave numbers from the four numerical approaches: (a) $k = 3$; (b) $k = 6$; (c) $k = 10$.

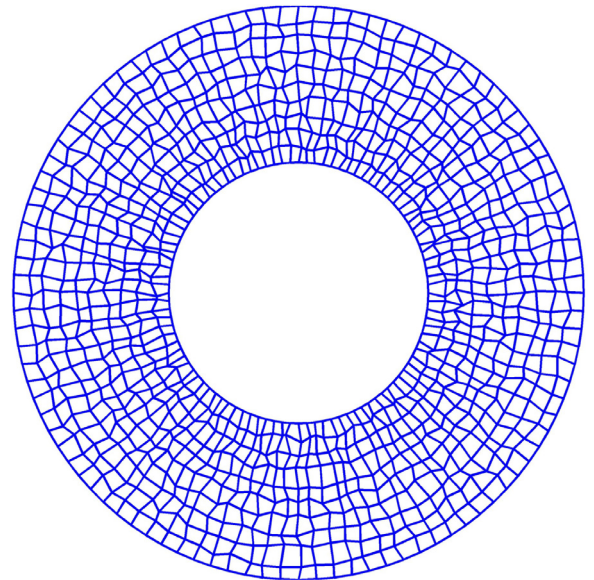


Fig. 9. The used irregular mesh for the involved problem domain.

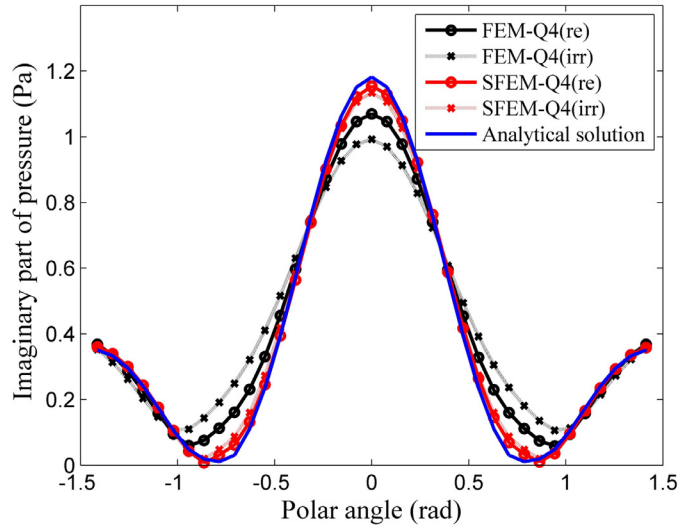


Fig. 10. The imaginary part of the scattered acoustic pressure results versus the polar angle for the regular mesh and the irregular mesh.

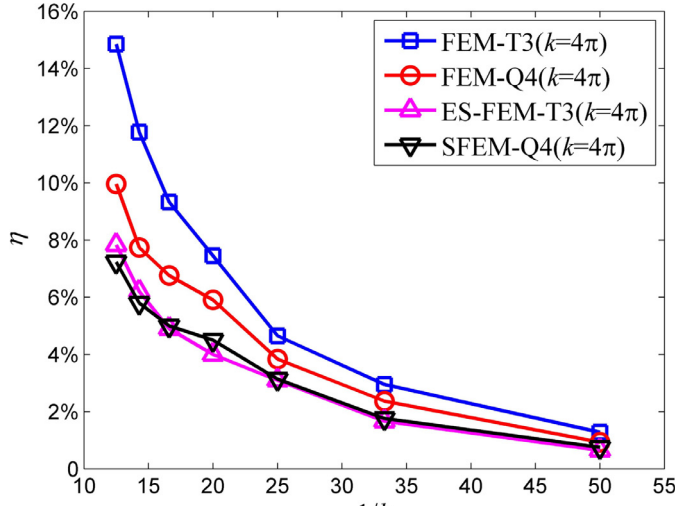
regular mesh (see Fig. 6) by using the following steps

$$x' = x + \Delta x \cdot r_c \cdot \beta \quad (45)$$

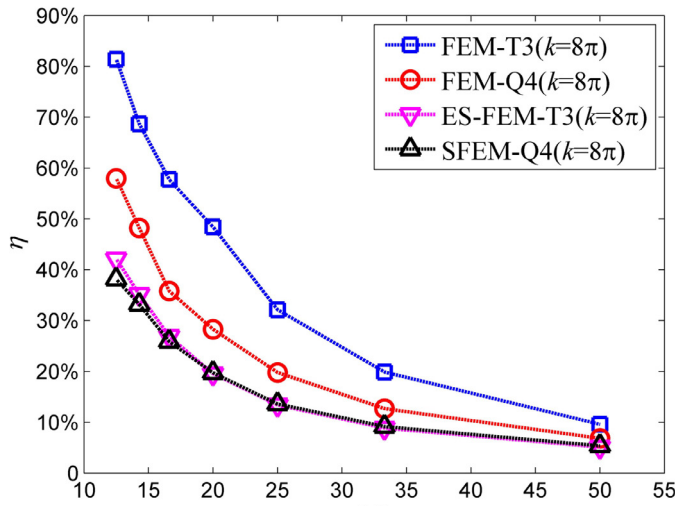
$$y' = y + \Delta y \cdot r_c \cdot \beta \quad (46)$$

where x and y represent the coordinate values of nodes for the initial regular mesh; x' and y' represent the corresponding values of nodes for the obtained irregular mesh; Δx and Δy denotes the average nodal space in the x - and y -directions, respectively; r_c are a series of random numbers and the corresponding values vary from -1 to 1 ; β stands for an so-called irregularity factor and its value is generally between 0 and 0.5 .

For a particular wave number $k = 8$, the forward scattering results for this problem will be computed and discussed here. Fig. 10 shows the imaginary part of the scattered acoustic pressure results at a distance of $R = 1$ from the center of the circular artificial boundary. With the aim to give a comparison, both the analytical solutions and the obtained numerical solutions (FEM-Q4 and SFEM-Q4) using regular mesh and irregular mesh are presented in the figure. From the results shown in the



(a)



(b)

Fig. 11. The relative numerical errors against the parameter $1/h$ at different wave numbers: (a) $k = 4\pi$; (b) $k = 8\pi$.

figure, it is easy to find that both the FEM-Q4 and SFEM-Q4 results will get worse if the used regular mesh is replaced by the irregular mesh. However, the accuracy of the FEM-Q4 results degrades much more than the corresponding SFEM-Q4 results if the irregular mesh is used. These important findings reveal that the present SFEM-Q4 is less sensitive to the mesh distortion than the standard FEM-Q4 and it can still work well even if the irregular mesh is used. The possible reason for this may be that the traditional coordinate transform process is not required in the formulation of the present SFEM-Q4 because only the shape function values at the quadrature points are needed to perform the involved numerical integration.

6.1.3. The convergence study

From the above analysis and discuss, it has been demonstrated that the performance of the present SFEM-Q4 is better than the original FEM-Q4 for acoustic scattering problems and the quality of the numerical solutions has been improved significantly using the identical node distri-

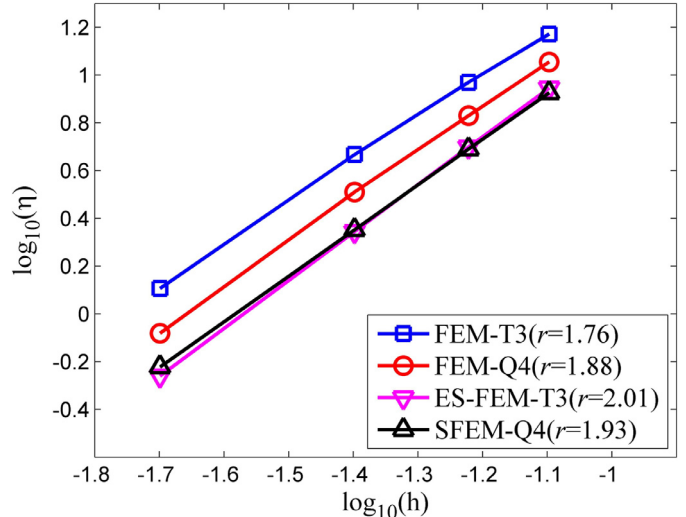


Fig. 12. The convergence rate of the different methods for the acoustic scattering problems.

butions. The convergence properties of the SFEM-Q4 for the Helmholtz problems will be further investigated in this sub-section. With the aim to perform the convergence study, several uniform mesh patterns with different average nodal space are employed here. Fig. 11 shows the relative numerical errors against the parameter $1/h$ (stands for the average nodal space). For the purpose of taking the influence of wave number into account, both the low wave number range ($k = 4\pi$) and the high wave number range ($k = 8\pi$) are considered here. In order to give a comparison, all the results from the four mentioned numerical approaches are presented in Fig. 11. The following vital findings can be found easily from the results shown in the figure.

(1) For any fixed mesh pattern, as the wave number values increases (from $k = 4\pi$ to $k = 8\pi$), the obtained relative numerical error results will get larger for all the several used numerical approaches. This is because the numerical error for high wave numbers is generally larger than that for low wave numbers. In addition, the ES-FEM-T3 behaves slightly better than the present SFEM-Q4; however, no matter in the high wave number range ($k = 8\pi$) or in the low wave number range ($k = 4\pi$), the relative numerical error results from ES-FEM-T3 and the present SFEM-Q4 are obviously smaller than the counters from the FEM-T3 and FEM-Q4. It is suggested that the numerical solutions from the present SFEM-Q4 are more accurate than those from the standard FEM (FEM-T3 and FEM-Q4) for acoustic scattering problems, and the performance of the original FEM-Q4 has been improved by the SFEM-Q4.

(2) As the quality of the employed mesh gets finer (the parameter $1/h$ get larger), the relative numerical error results from all the numerical approaches will trend to zero for both low wave number value and high wave number value. However, compared to the FEM-T3 and FEM-T4 results, the ES-FEM-T3 and SFEM-Q4 results evidently converge faster. It is verified that the SFEM-Q4 is the same as the ultra-convergent ES-FEM-T3 which has been proved in the previous published paper [60], and possesses better convergence properties than the FEM-T3 and FEM-Q4 for the acoustic scattering problems because the original “overly-stiff” numerical model has been properly softened by the used gradient smoothing technique (GST) and then the stiffness of the obtained numerical model is much closer to the exact one.

Furthermore, with the aim to study the convergence property of the SFEM-Q4 more clearly, for the fixed wave number $k = 4\pi$, the convergence rate results for four different numerical approaches are also calculated and discussed here (see Fig. 12). From Fig. 12, it is found that

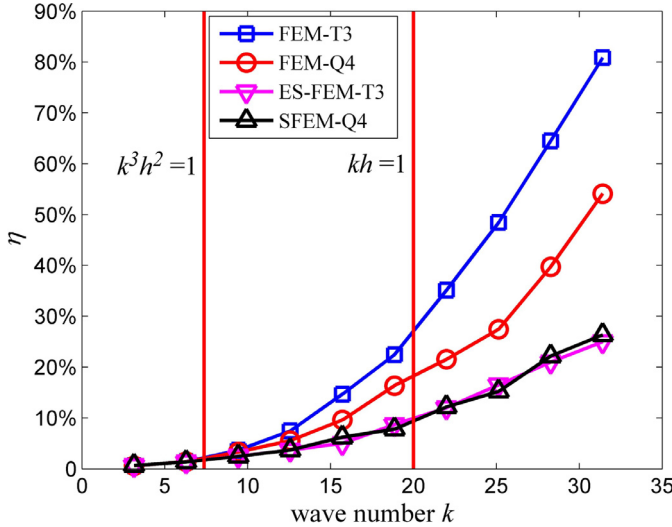


Fig. 13. The relative numerical error results against the wave number k for the different numerical approaches.

the convergence rate of the ES-FEM-T3 ($r = 2.01$) is the fastest, however, the convergence behavior of the present SFEM-Q4 ($r = 1.93$) is still better than the FEM-Q4 ($r = 1.88$) and FEM-T3 ($r = 1.73$). These findings indicate that the convergence behavior of present SFEM-Q4 ($r = 1.93$) is not as good as the ES-FEM-T3, which has been proved to be a very effective numerical method for acoustic scattering problems; however, the SFEM-Q4 still possesses faster convergence rate property than the FEM-Q4 and FEM-T3.

6.1.4. The control of the numerical error

As presented in Section 5, the relative numerical error of the classical finite element solutions for the Helmholtz equation consists of two different parts, namely the interpolation error component and the pollution error component. The interpolation error is associated with the parameter kh and the pollution error is associated with the parameter k^3h^2 . The related parameters kh and k^3h^2 are also called the pre-asymptotic and asymptotic estimate in several published literatures. The numerical error issue for the Helmholtz problem has been recognized as a well-known unsolved problem for current existent computational methods [63]. For the past few decades, a lot of efforts has been made by the researchers to handle the numerical error for the acoustics governed by the Helmholtz equation, however, the numerical error only can be suppressed to some small extent and cannot be avoided completely by the modern numerical techniques. In this sub-section, the ability of the present SFEM-Q4 and the other numerical approaches in repressing the numerical error for acoustic scattering problems will be compared and investigated. In order to perform the study of the numerical error estimate clearly, both the quality of the used mesh patterns and the wave number k are taken into consideration here. First, the related study will be carried out for a fixed mesh pattern. Fig. 13 plots the relative numerical error results against the wave number k for the above-mentioned acoustic scattering problem. To give a comparison, all the results from the four different numerical approaches are depicted in the figure. For the convenience of discuss and analysis, both the pre-asymptotic ($kh = 1$) and asymptotic ($k^3h^2 = 1$) are also shown in Fig. 13. From the data shown in Fig. 13, it is clear that the following fundamental findings can be obtained:

- (1) At small wave number values ($k^3h^2 < 1$), the relative numerical error results are in relatively low level for all the four numerical approaches. This is because the numerical error is mainly from the interpolation error component and it is very small for low wave number range.

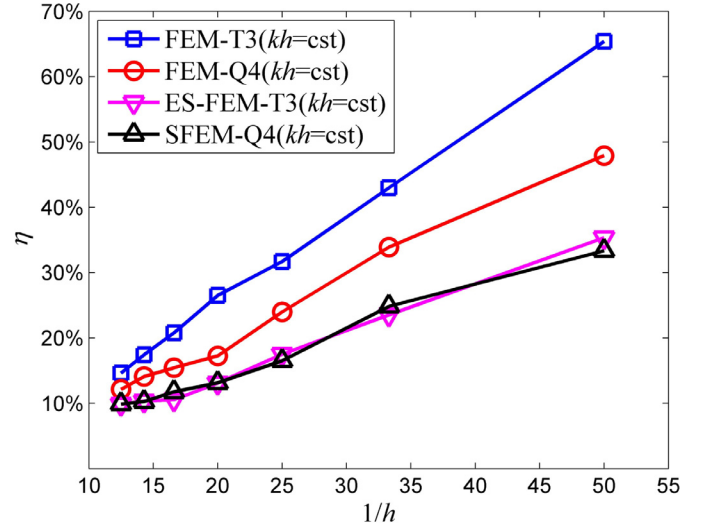


Fig. 14. The relative numerical error results from the four numerical approaches against the parameter $1/h$ in the case of keeping $kh = \text{constant}$.

- (2) As the value of the wave number increases, the relative numerical error results will grow evidently and quickly. The reason for this is that the pollution error component will dominate the numerical error and it is generally much larger than the interpolation error at relatively large wave number range ($kh > 1$).
- (3) In the overall performance, the present SFEM-Q4 is a good competitor to the ES-FEM-T3 and is obviously superior to the other two standard FEM models. It is suggested that the ability of the original FEM-Q4 in controlling the numerical error for acoustic problems has been synergized by the present SFEM-Q4 due to the related gradient smoothing operations.

Then the relative numerical error assessment for acoustic scattering problems will be carried out by considering a series of mesh patterns with different average nodal spaces. Fig. 14 gives the relative numerical error results from the four numerical approaches against the parameter $1/h$ by varying the value of the wave number k and keeping $kh = \text{constant}$. The results shown in the figure reveal that the relative numerical error will increase linearly with the wave number k in the case of keeping $kh = \text{constant}$. This is because the interpolation error for the Helmholtz problems, which is exactly equivalent to the numerical error of the finite element solutions for standard elasticity problems, is local in nature and it will converge in the same rate if the quality of the used meshes gets finer [64]. However, another kind of the numerical error component (i.e. the pollution error), which is associated with the parameter k^3h^2 , cannot be suppressed by keeping $kh = \text{constant}$.

As opposed to the interpolation error, the pollution error is a new error component in the framework of the Helmholtz problems. It is global in nature and will converge in the different rate (much slower than the interpolation error) when the used meshes get more refined. From the expression presented in Eq. (42) and Eq. (43), it is clear that the pollution error component has an additional dependence on the wave number k compared to the interpolation error component and only keeping $kh = \text{constant}$ is not sufficient to control the total numerical error. Therefore, it is not difficult to understand the phenomenon found in Fig. 14 because the pollution error component will still increase linearly even though the interpolation error component has been controlled by keeping $kh = \text{constant}$. In addition, it is worth noting that the above analysis about the numerical error for Helmholtz problems also gives the reasons why the traditional “rules of thumb” (i.e. keeping $kh = \text{constant}$) is not sufficient to suppress the numerical error well for large wave number range.

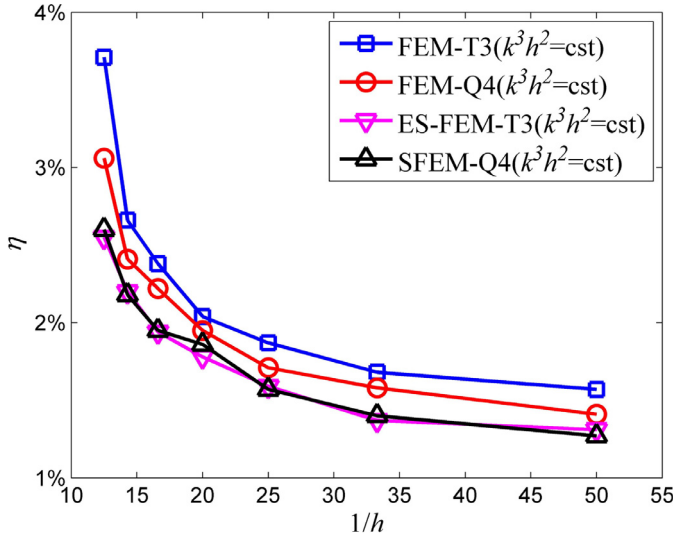


Fig. 15. The relative numerical error results from the four numerical approaches against the parameter $1/h$ in the case of keeping $k^3 h^2 = \text{constant}$.

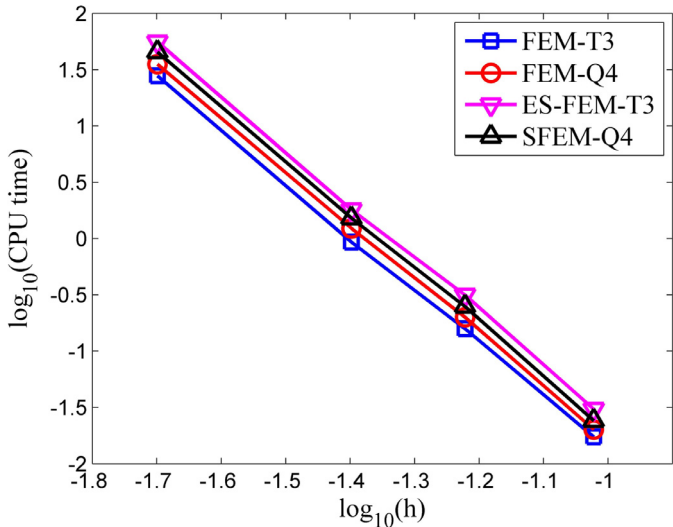


Fig. 16. The computational cost versus the average mesh size for the different numerical methods.

Furthermore, the relative numerical error for all the four numerical approaches are computed and discussed by varying the wave number k and keeping $k^3 h^2 = \text{constant}$. The corresponding numerical results are plotted in Fig. 15. It is shown that the relative numerical error can be well controlled by keeping $k^3 h^2 = \text{constant}$ because both the interpolation error component and the pollution error component can be suppressed if $k^3 h^2 = \text{constant}$ is kept. More importantly, it should be pointed out that the present SFEM-Q4 has the similar ability as the ES-FEM-T3 in controlling the numerical error, and it is evidently much better than the FEM-T3 and FEM-Q4, no matter in the case of keeping $kh = \text{constant}$ (see Fig. 14) or in the case of keeping $k^3 h^2 = \text{constant}$ (see Fig. 15). It is indicated that the present SFEM-Q4 and ES-FEM-T3 surpass the FEM-T3 and FEM-Q4 in analyzing the acoustic scattering problems.

6.1.5. The computational efficiency study

From the above comparison and discuss in the previous section, it is known that the performance of the original FEM-Q4 for acoustic scattering problems has been significantly improved by the present SFEM-Q4 and the SFEM-Q4 shows more excellent ability in controlling the relative numerical error for the Helmholtz problems. However, the good

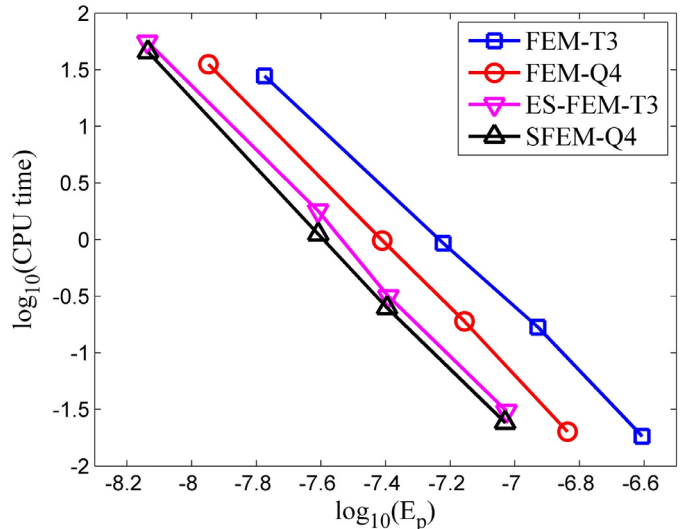


Fig. 17. The consuming CPU time against the numerical error indicator for the different numerical approaches.

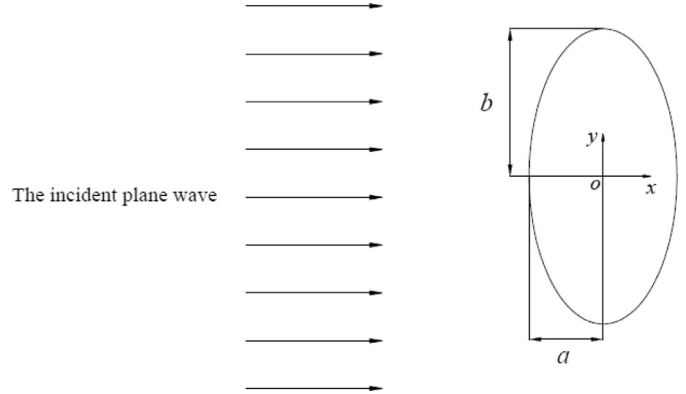
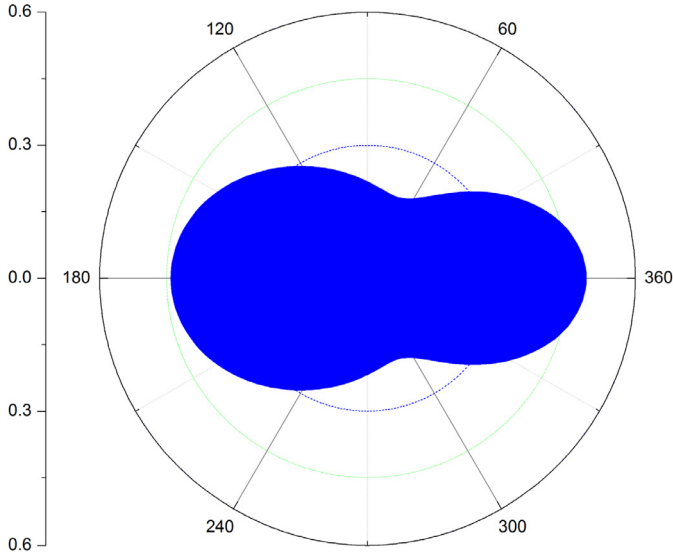


Fig. 18. The schematic description of the numerical model for the elliptical cylinder.

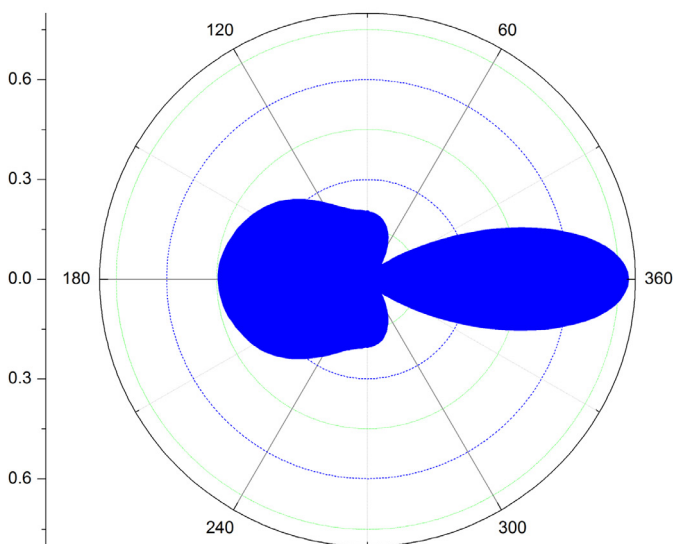
features of the SFEM-Q4 are not free of any price. In the process of formulating the present SFEM-Q4 and performing the gradient smoothing operations, the extra computational cost is needed because some pre-processing operations (obtaining the smoothing domains) are necessary. Actually, more consuming CPU time (s) is required for SFEM-Q4 than the original FEM-Q4 if the identical node distribution is used. Therefore, whether or not the present SFEM-Q4 is more numerically effective for the acoustic scattering problems is still unclear.

In this sub-section, the computational efficiency of the above-mentioned numerical methods (FEM-T3, FEM-Q4, ES-FEM-T3 and SFEM-Q4) will be compared and discussed. With the aim to carry out the computational efficiency study, all the programs are compiled in the same hardware configuration and several mesh patterns with different average nodal spaces are employed here. For the fixed wave number $k = 8$, the computational cost for the different numerical methods (see Fig. 16) is calculated and discussed first. From the figure, it is seen that the two SFEMs (SFEM-Q4 and ES-FEM-T3) are clearly more expensive than the two standard FEMs (FEM-Q4 and FEM-T3), this is because the related pre-processing operations and gradient smoothing operations indeed increase the computational cost. In addition, it is also seen that the ES-FEM-T3 needs more computational cost than the present SFEM-Q4, the reason for this is that the bandwidth of the system matrix for SFEM-Q4 is always smaller than the ES-FEM-T3 with the same node distributions.

Moreover, Fig. 17 depicts the consuming CPU time (s) against the numerical error indicator for the four different numerical approaches.



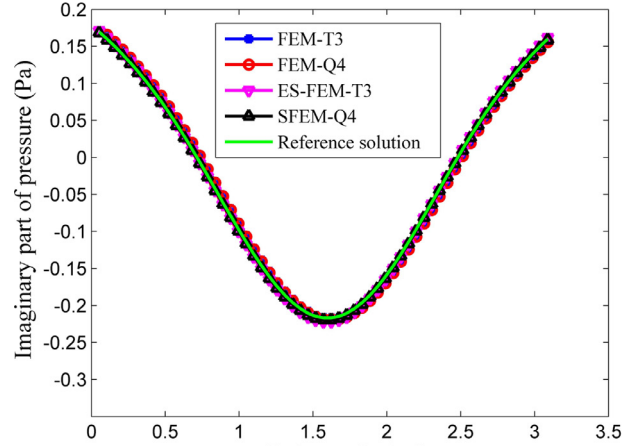
(a)



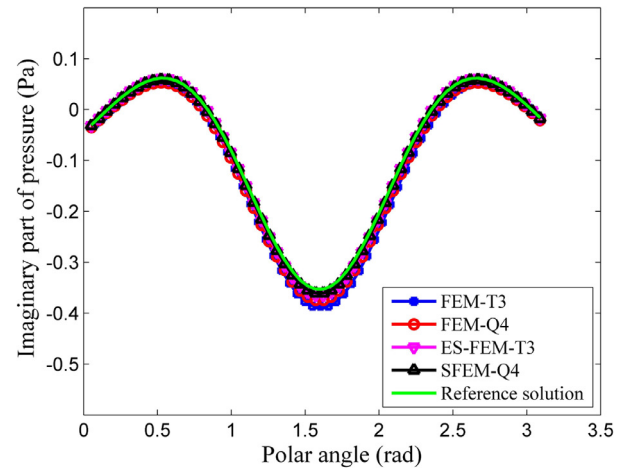
(b)

Fig. 19. The scattering pattern results obtained from the present SFEM-Q4 for the elliptical cylinder: (a) $k = 10$; (b) $k = 25$.

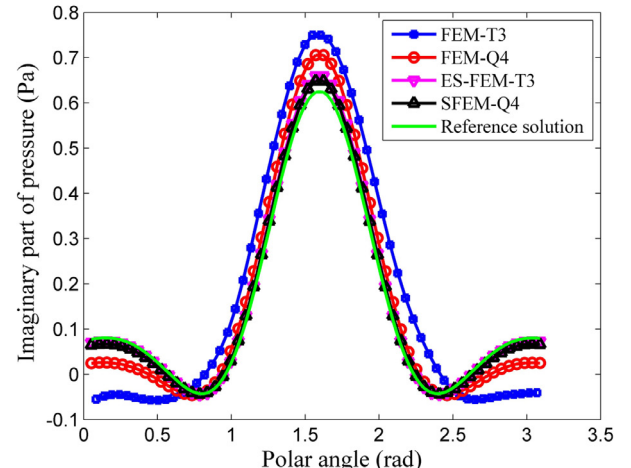
From the results shown in the figure, it is clear that though the two SFEMs need more CPU (s) time than the two standard FEMs, however, if the numerical error indicator is taken into account, the SFEMs usually possess the higher computational efficiency with the same node distributions for the acoustic scattering problems. In other words, much less computational cost for SFEMs is required than the standard FEMs for the same accuracy of numerical solutions. More importantly, it should be pointed that the present SFEM-Q4 even possesses the higher computational efficiency than the ES-FEM-T3. This suggests that the present SFEM-Q4 is a very good alternative to the ES-FEM-T3 and could provide fairly reliable numerical solutions for the acoustic scattering problems even though relatively coarse meshes are employed.



(a)



(b)



(c)

Fig. 20. The imaginary part of the scattered acoustic pressure results versus the polar angle for the elliptical cylinder: (a) $k = 8$; (b) $k = 16$; (c) $k = 24$.

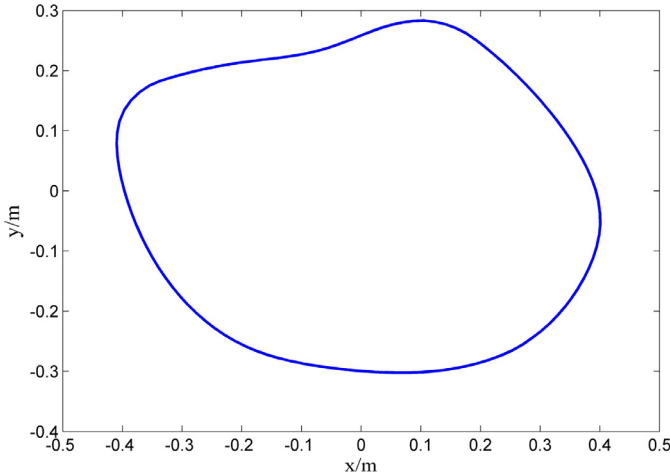


Fig. 21. The acoustic scattering by the object with arbitrary shape.

6.2. The acoustic scattering by infinite cylinder with elliptical section

The second numerical example considered here is the plane acoustic wave scattering by an infinite cylinder with elliptical section. The schematic description of the numerical model is given in Fig. 18. The aspect ratio of the elliptical scatterer is $a/b = 0.5$ ($a = 0.1$ and $b = 0.2$). The remaining boundary conditions and material parameters are unchanged from the numerical example considered in the previous section. The involved problem domain is discretized into quadrilateral elements and triangular elements and the average nodal space is 0.04. The scattering pattern results at different wave numbers ($k = 10$ and $k = 25$) obtained from the present SFEM-Q4 for this numerical example are presented in Fig. 19. The results shown in the figures reveal that the present SFEM-Q4 solutions for the acoustic scattering by elliptical cylinder are in very good agreement with the solutions from the partial wave series expansions (PWSE) technique [1]. Therefore, it can be concluded that the present SFEM-Q4 is sufficiently feasible and effective to handle the acoustic scattering problems.

With the aim to further investigate the acoustic scattered field obtained from the present SFEM-Q4 and test the performance of SFEM-Q4 more detailedly, the imaginary part of the scattered acoustic pressure results at a distance of $R = 1$ m from the center of the circular artificial boundary are also calculated and compared here. The corresponding numerical results at three different wave numbers ($k = 8$, $k = 16$ and $k = 24$) from all the four approaches are depicted in Fig. 20. For comparison, the reference solutions from the FEM-T3 with very refined mesh pattern are also presented in the figures. Again, it is clearly seen that all the numerical solutions have similar accuracy and agree well with reference solutions at small wave number ($k = 8$). As the considered wave number values get larger ($k = 16$ and $k = 24$), their individual performance will be different each other; although the present SFEM-Q4 solutions are very close to the ES-FEM-T3 and these two SFEMs almost have the same computational accuracy, however, the SFEM-Q4 clearly behaves better than the FEM-T3 and FEM-Q4, and the obtained numerical solutions are obviously closer to the reference solutions. These findings are even more striking in the large wave number range ($k = 24$). This numerical example again reveals that the present SFEM-Q4 has evident advantages over the original FEM-Q4 in solving the acoustic scattering problems, especially in large wave number values.

6.3. The acoustic scattering by the object with arbitrary shape

In this section, a more realistic and complicated acoustic scattering problem will be considered. The illustration of this numerical example is shown in Fig. 21. All the boundary conditions and material parameters are retained and the quadrilateral and triangular elements with

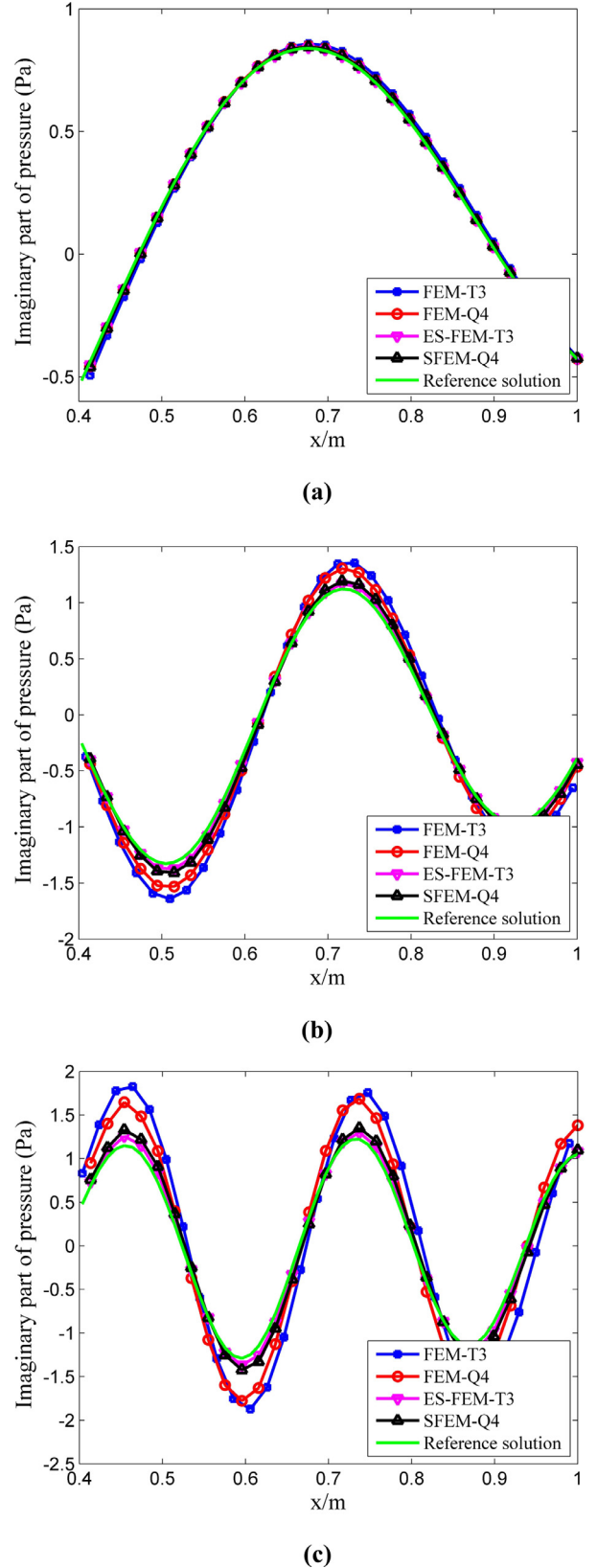


Fig. 22. The imaginary part of the scattered pressure at different wave number values along the x -axis for the object with arbitrary shape: (a) $k = 8$; (b) $k = 16$; (c) $k = 24$.

average nodal space 0.025 are used to divide the involved problem domain. Likewise, the imaginary part of the scattered pressure at different wave number values ($k = 8$, $k = 16$ and $k = 24$) along the x -axis are computed and discussed here. The obtained numerical results from different numerical approaches are plotted in Fig. 22. To give a comparison, the corresponding numerical solutions from the FEM-T3 with extremely refined mesh are also presented here as the reference solutions. The results plotted in the figures show that the obtained findings and conclusions are very similar as those obtained from the previous numerical examples. This realistic acoustic scattering problem again demonstrates that the present SFEM-Q4 behaves better than the original FEM-Q4 in analyzing the acoustic scattering and more accurate and reliable numerical solutions can be obtained by the SFEM-Q4, in particular for large wave number values.

7. Conclusions

In this work, a smoothed finite element method with quadrilateral elements (SFEM-Q4) is proposed to handle the acoustic wave scattering by underwater objects. Several typical numerical examples are conducted to demonstrate the validity and feasibility of the present SFEM-Q4 for underwater acoustic scattering problems. From the obtained numerical solutions, the following conclusions could be drawn:

- (1) Owing to the softening effects provided by the gradient smoothing technique (GST), the present SFEM-Q4 possesses more appropriate stiffness of the continuous system than the original FEM-Q4 and more accurate and reliable numerical solutions can be obtained for the underwater acoustic scattering problems.
- (2) Due to the better performance of the present SFEM-Q4 than the original FEM-Q4, the traditional requirement of at least six elements should be used to resolve a wavelength can be relaxed to some extent and the present SFEM-Q4 can provide fairly reliable numerical solutions even if the relatively coarse meshes are employed.
- (3) Since the conventional coordinate transform program is not required in the process of performing the numerical integration, the present SFEM-Q4 works better with distorted meshes than the original FEM-Q4 for acoustic scattering problems.
- (4) The present SFEM-Q4 possesses more excellent performance than the FEM-T3 and FEM-Q4 in controlling the numerical error and is shown to be a very good competitor and alternative to the ultra-convergent ES-FEM-T3 for the acoustic scattering problems.
- (5) The SFEM-Q4 is presented for two dimensions in this paper and can be generalized in three dimensions. Due to the good properties, it is very promising to extend the application of the present SFEM-Q4 to more complicated and realistic acoustic scattering problems.

Acknowledgment

The authors wish to express their gratitude to the National Natural Science Foundation of China (contract nos. 51579112, 51379083 and 51579109).

References

- [1] Mitri FG. Resonance scattering and radiation force calculations for an elastic cylinder using the translational addition theorem for cylindrical wave functions. *AIP Adv* 2015;5:097205.
- [2] DiPerna DT, Stanton TK. Sound scattering by cylinders of noncircular cross section: a conformal mapping approach. *J Acoust Soc Am* 1994;96:3064–79.
- [3] Gong ZX, Li W, Mitri FG, Chai YB, Zhao Y. Arbitrary scattering of an acoustical Bessel beam by a rigid spheroid with large aspect-ratio. *J Sound Vib* 2016;383:233–47.
- [4] Gong ZX, Li W, Chai YB, Zhao Y, Mitri FG. T-matrix method for acoustical Bessel beam scattering from a rigid finite cylinder with spheroidal endcaps. *Ocean Eng* 2017;129:507–19.
- [5] Harari I, Hughes TJR. Galerkin/least-squares finite element methods for the reduced wave equation with non-reflecting boundary conditions in unbounded domains. *Comput Methods Appl Mech Eng* 1992;98:411–54.
- [6] Fu ZJ, Chen W, Gu Y. Burton–Miller-type singular boundary method for acoustic radiation and scattering. *J Sound Vib* 2014;333:3776–93.
- [7] Fu ZJ, Chen W, Lin J, Cheng AHD. Singular boundary method for various exterior wave applications. *Int J Comput Methods* 2015;12:1550011.
- [8] Li JP, Chen W, Fu ZJ, Sun LL. Explicit empirical formula evaluating original intensity factors of singular boundary method for potential and Helmholtz problems. *Eng Anal Bound Elem* 2016;73:161–9.
- [9] Chen W, Wang F. Singular boundary method using time-dependent fundamental solution for transient diffusion problems. *Eng Anal Bound Elem* 2016;68:115–23.
- [10] Ihlenburg F, Babuška I, Sauter S. Reliability of finite element methods for the numerical computation of waves. *Adv Eng Softw* 1997;28:417–24.
- [11] Babuška I, Ihlenburg F, Paik ET, Sauter SA. A generalized finite element method for solving the Helmholtz equation in two dimensions with minimal pollution. *Comput Methods Appl Mech Eng* 1995;128:325–59.
- [12] Wenterodt C, Estorff O. Dispersion analysis of the meshfree radial point interpolation method for the Helmholtz equation. *Int J Numer Methods Eng* 2009;77:1670–89.
- [13] Bouillard P, Suleaub S. Element-free Galerkin solutions for Helmholtz problems: formulation and numerical assessment of the pollution effect. *Comput Methods Appl Mech Eng* 1998;162:317–35.
- [14] He ZC, Liu GR, Zhong ZH, Wu SC, Zhang GY, Cheng AG. An edge-based smoothed finite element method (ES-FEM) for analyzing three-dimensional acoustic problems. *Comput Methods Appl Mech Eng* 2009;199:20–33.
- [15] Chen M, Li M, Liu GR. Mathematical basis of G spaces. *Int J Comput Methods* 2016;13:1641007.
- [16] Liu GR, Zhang GY. Smoothed point interpolation methods: G space theory and weakened weak forms. World Scientific; 2013.
- [17] Zhang GY, Li Y, Gao XX, Hui D, Wang SQ, Zong Z. Smoothed point interpolation method for elastoplastic analysis. *Int J Comput Methods* 2015;12:1540013.
- [18] Wu G, Zhang J, Li Y, Yin L, Liu Z. Analysis of transient thermo-elastic problems using a cell-based smoothed radial point interpolation method. *Int J Comput Methods* 2016;13:1650023.
- [19] Zhang GY, Li Y, Wang HY, Gu YT, Zong Z. A linear complementarity formulation of meshfree method for elastoplastic analysis of gradient-dependent plasticity. *Eng Anal Bound Elem* 2016;73:1–13.
- [20] Zhang GY, Wittek A, Joldes GR, Jin X, Miller K. A three-dimensional nonlinear mesh-free algorithm for simulating mechanical responses of soft tissue. *Eng Anal Bound Elem* 2014;42:60–6.
- [21] Feng SZ, Cui XY, Chen F, Liu SZ, Meng DY. An edge/face-based smoothed radial point interpolation method for static analysis of structures. *Eng Anal Bound Elem* 2016;68:1–10.
- [22] Liu GR, Nguyen-Thoi T, Dai KY, Lam KY. Theoretical aspects of the smoothed finite element method (SFEM). *Int J Numer Meth Eng* 2007;71:902–30.
- [23] Nguyen-Xuan H, Bordas S, Nguyen-Dang H. Smooth finite element methods: convergence, accuracy and properties. *Int J Numer Meth Eng* 2008;74:175–208.
- [24] Li W, Chai YB, Lei M, Liu GR. Analysis of coupled structural-acoustic problems based on the smoothed finite element method (S-FEM). *Eng Anal Bound Elem* 2014;42:84–91.
- [25] Zeng W, Liu GR, Jiang C, Nguyen-Thoi T, Jiang Y. A generalized beta finite element method with coupled smoothing techniques for solid mechanics. *Eng Anal Bound Elem* 2016;73:103–19.
- [26] Zeng W, Liu GR. Smoothed finite element methods (S-FEM): an overview and recent developments. *Arch Comput Method Eng* 2016;1:1–39 <https://link.springer.com/article/10.1007/s11831-016-9202-3>.
- [27] Chai YB, Li W, Gong ZX, Li TY. Hybrid smoothed finite element method for two dimensional acoustic radiation problems. *Appl Acoust* 2016;103:90–101.
- [28] Wan DT, Hu D, Yang G, Long T. A fully smoothed finite element method for analysis of axisymmetric problem. *Eng Anal Bound Elem* 2016;72:78–88.
- [29] Cui XY, Hu XB, Li GY, Liu GR. A modified smoothed finite element method for static and free vibration analysis of solid mechanics. *Int J Comput Methods* 2016;3:1650043.
- [30] Chai YB, Li W, Liu GR, Li TY, Gong ZX. A superconvergent alpha finite element method (SaFEM) for static and free vibration analysis of shell structures. *Comput Struct* 2017;179:27–47.
- [31] Liu GR, Gu YT. A point interpolation method for two-dimensional solids. *Int J Numer Meth Eng* 2001;50:937–51.
- [32] Xu X, Zheng ZQ, Gu YT, Liu GR. A quasi-conforming point interpolation method (QC-PIM) for elasticity problems. *Int J Comput Methods* 2016;13:1650026.
- [33] Liu MB, Liu GR. Smoothed particle hydrodynamics—a meshfree particle method. World Scientific; 2003.
- [34] Zhang YO, Zhang T, Ouyang H, Li TY. Efficient SPH simulation of time-domain acoustic wave propagation. *Eng Anal Bound Elem* 2016;62:112–22.
- [35] Zhang YO, Zhang T, Ouyang H, Li TY. SPH simulation of acoustic waves: effects of frequency, sound pressure, and particle spacing. *Math Probl Eng* 2015. doi:10.1155/2015/348314.
- [36] Liu GR. An overview on meshfree methods: for computational solid mechanics. *Int J Comput Methods* 2016;13:1630001.
- [37] Liu GR, Nguyen-Thoi T, Nguyen-Xuan H, Lam KY. A node-based smoothed finite element method (NS-FEM) for upper bound solutions to solid mechanics problems. *Comput Struct* 2009;87:14–26.
- [38] Nguyen-Thoi T, Vu-Do HC, Rabczuk T, Nguyen-Xuan H. A node-based smoothed finite element method (NS-FEM) for upper bound solution to visco-elastoplastic analyses of solids using triangular and tetrahedral meshes. *Comput Methods Appl Mech Eng* 2010;199:3005–27.
- [39] Nguyen-Thoi T, Phung-Van P, Rabczuk T, Nguyen-Xuan H, Le-Van C. An application of the ES-FEM in solid domain for dynamic analysis of 2D fluid–solid interaction problems. *Int J Comput Methods* 2013;10:1340003.

- [40] Feng H, Cui XY, Li GY. A stable nodal integration method with strain gradient for static and dynamic analysis of solid mechanics. Eng Anal Bound Elem 2016;62:78–92.
- [41] Liu GR, Chen M, Li M. Lower bound of vibration modes using the node-based smoothed finite element method (NS-FEM). Int J Comput Methods 2017;14:1750036.
- [42] Nguyen-Xuan H, Liu GR, Thai-Hoang CA, Nguyen-Thoi T. An edge-based smoothed finite element method (ES-FEM) with stabilized discrete shear gap technique for analysis of Reissner–Mindlin plates. Comput Methods Appl Mech Eng 2010;199:471–89.
- [43] Nguyen-Xuan H, Tran LV, Nguyen-Thoi T, Vu-Do HC. Analysis of functionally graded plates using an edge-based smoothed finite element method. Compos Struct 2011;93:3019–39.
- [44] Phung-Van P, Thai CH, Nguyen-Thoi T, Nguyen-Xuan H. Static and free vibration analyses of composite and sandwich plates by an edge-based smoothed discrete shear gap method (ES-DSG3) using triangular elements based on layerwise theory. Compos Pt B—Eng 2014;60:227–38.
- [45] Cui XY, Chang S, Li G Y. A two-step Taylor Galerkin smoothed finite element method for Lagrangian dynamic problem. Int J Comput Methods 2015;12:1540004.
- [46] Cui XY, Chang S. Edge-based smoothed finite element method using two-step Taylor Galerkin algorithm for Lagrangian dynamic problems. Int J Comput Methods 2015;12:1550028.
- [47] Chai YB, Li W, Li TY, Gong ZX, You XY. Analysis of underwater acoustic scattering problems using stable node-based smoothed finite element method. Eng Anal Bound Elem 2016;72:27–41.
- [48] Hu XB, Cui XY, Feng H, Li GY. Stochastic analysis using the generalized perturbation stable node-based smoothed finite element method. Eng Anal Bound Elem 2016;70:40–55.
- [49] Zeng W, Liu GR, Jiang C, Dong XW, Chen HD, Bao Y, et al. An effective fracture analysis method based on the virtual crack closure-integral technique implemented in CS-FEM. Appl Math Model 2016;40:3783–800.
- [50] Yang YT, Zheng H, Du XL. An enriched edge-based smoothed FEM for linear elastic fracture problems. Int J Comput Methods 2016;14:1750052.
- [51] Nguyen-Thoi T, Rabczuk T, Ho-Huu V, Le-Anh L, Dang-Trung H, Vo-Duy T. An extended cell-based smoothed three-node Mindlin plate element (XCS-MIN3) for free vibration analysis of cracked FGM plates. Int J Comput Methods 2017;14:1750011.
- [52] Jiang C, Zhang ZQ, Liu GR, Han X, Zeng W. An edge-based/node-based selective smoothed finite element method using tetrahedrons for cardiovascular tissues. Eng Anal Bound Elem 2015;59:62–77.
- [53] He ZC, Liu GR, Zhong ZH, Cui XY, Zhang GY, Cheng AG. A coupled edge-/face-based smoothed finite element method for structural-acoustic problems. Appl Acoust 2010;71:955–64.
- [54] Wang G, Cui XY, Liang ZM, Li GY. A coupled smoothed finite element method (S-FEM) for structural-acoustic analysis of shells. Eng Anal Bound Elem 2015;61:207–17.
- [55] He ZC, Liu GR, Zhong ZH, Zhang GY, Cheng AG. A coupled ES-FEM/BEM method for fluid-structure interaction problems. Eng Anal Bound Elem 2011;35:140–7.
- [56] Gong ZX, Chai YB, Li W. Coupled analysis of structural-acoustic problems using the cell-based smoothed three-node Mindlin plate element. Int J Comput Methods 2016;13:1640007.
- [57] Chai YB, Li W, Gong ZX, Li TY. Hybrid smoothed finite element method for two-dimensional underwater acoustic scattering problems. Ocean Eng 2016;116:129–41.
- [58] Hu X, Cui XY, Zhang Q, Wang G, Li GY. The stable node-based smoothed finite element method for analyzing acoustic radiation problems. Eng Anal Bound Elem 2017;80:142–51.
- [59] Wang G, Cui XY, Liang ZM, Li GY. A coupled smoothed finite element method (S-FEM) for structural-acoustic analysis of shells. Eng Anal Bound Elem 2015;61:207–17.
- [60] Li W, Chai YB, Lei M, Li TY. Numerical investigation of the edge-based gradient smoothing technique for exterior Helmholtz equation in two dimensions. Comput Struct 2017;182:149–64.
- [61] Wu F, Yao LY, Hu M, He ZC. A stochastic perturbation edge-based smoothed finite element method for the analysis of uncertain structural-acoustics problems with random variables. Eng Anal Bound Elem 2017;80:116–26.
- [62] Keller JB, Givoli D. Exact non-reflecting boundary conditions. J Comput Phys 1989;82:172–92.
- [63] Zienkiewicz OC. Achievements and some unsolved problems of finite element method. Int J Numer Methods Eng 2000;47:8–28.
- [64] Steffens LM, Parés N, Díez P. Estimation of the dispersion error in the numerical wave number of standard and stabilized finite element approximations of the Helmholtz equation. Int J Numer Meth Eng 2011;86:1197–224.